IEC TS 62607-9-2

Edition 1.0 2024-07

TECHNICAL SPECIFICATION

colour inside

Nanomanufacturing – Key control characteristics – Part 9-2: Nanomagnetic products – Magnetic field distribution: Magneto-optical indicator film technique

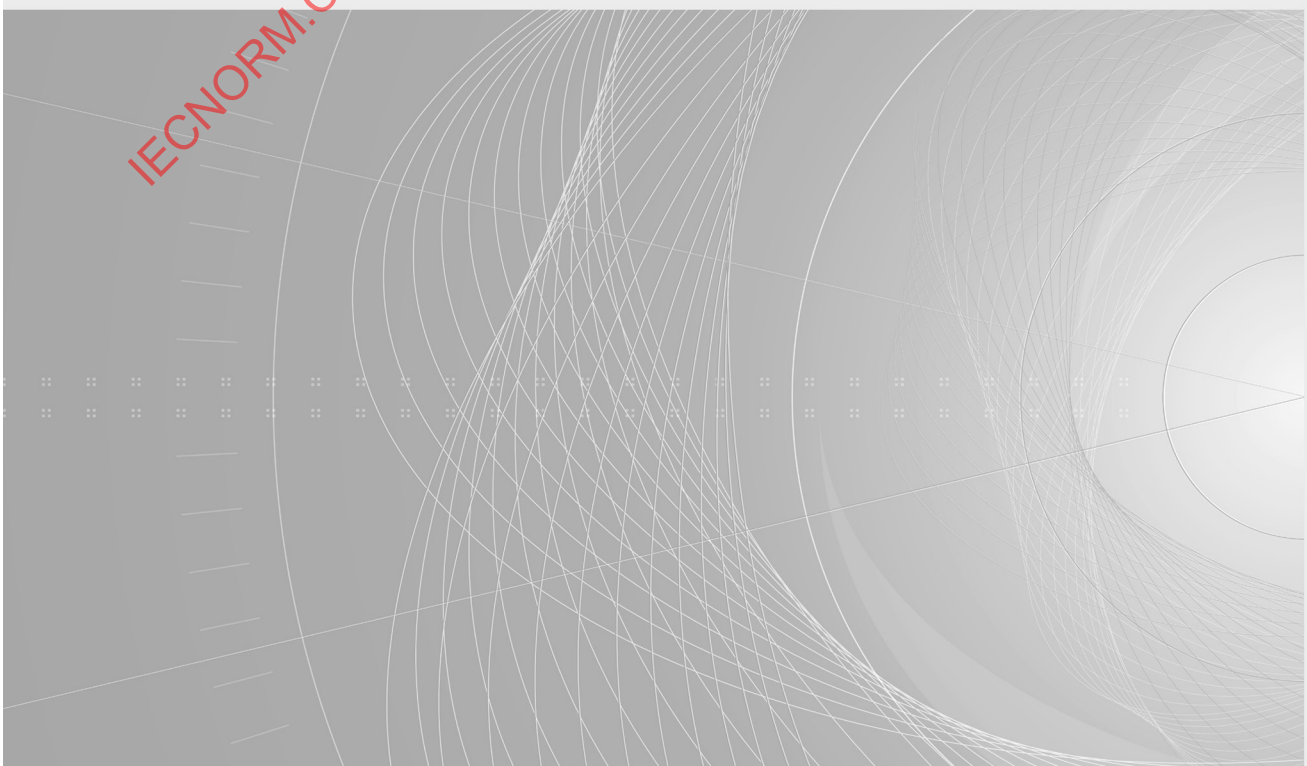

IEC TS 62607-9-2:2024-07(en)

IEC Secretariat
3, rue de Varembé
CH-1211 Geneva 20
Switzerland

Tel.: +41 22 919 02 11
info@iec.ch
www.iec.ch

About the IEC
The International Electrotechnical Commission (IEC) is the leading global organization that prepares and publishes International Standards for all electrical, electronic and related technologies.

About IEC publications
The technical content of IEC publications is kept under constant review by the IEC. Please make sure that you have the latest edition, a corrigendum or an amendment might have been published.

IEC publications search - webstore.iec.ch/advsearchform
The advanced search enables to find IEC publications by a variety of criteria (reference number, text, technical committee, …). It also gives information on projects, replaced and withdrawn publications.

IEC Just Published - webstore.iec.ch/justpublished
Stay up to date on all new IEC publications. Just Published details all new publications released. Available online and once a month by email.

IEC Customer Service Centre - webstore.iec.ch/csc
If you wish to give us your feedback on this publication or need further assistance, please contact the Customer Service Centre: sales@iec.ch.

IEC Products & Services Portal - products.iec.ch
Discover our powerful search engine and read freely all the publications previews, graphical symbols and the glossary. With a subscription you will always have access to up to date content tailored to your needs.

Electropedia - www.electropedia.org
The world's leading online dictionary on electrotechnology, containing more than 22 500 terminological entries in English and French, with equivalent terms in 25 additional languages. Also known as the International Electrotechnical Vocabulary (IEV) online.

IEC TS 62607-9-2

Edition 1.0 2024-07

TECHNICAL SPECIFICATION

Nanomanufacturing – Key control characteristics – Part 9-2: Nanomagnetic products – Magnetic field distribution: Magneto-optical indicator film technique

INTERNATIONAL ELECTROTECHNICAL COMMISSION

ICS 07.120

ISBN 978-2-8322-8987-7

CONTENTS

INTERNATIONAL ELECTROTECHNICAL COMMISSION

_____

NANOMANUFACTURING – KEY CONTROL CHARACTERISTICS –

Part 9-2: Nanomagnetic products – Magnetic field distribution: Magneto-optical indicator film technique

FOREWORD

1) The International Electrotechnical Commission (IEC) is a worldwide organization for standardization comprising all national electrotechnical committees (IEC National Committees). The object of IEC is to promote international co-operation on all questions concerning standardization in the electrical and electronic fields. To this end and in addition to other activities, IEC publishes International Standards, Technical Specifications, Technical Reports, Publicly Available Specifications (PAS) and Guides (hereafter referred to as "IEC Publication(s)"). Their preparation is entrusted to technical committees; any IEC National Committee interested in the subject dealt with may participate in this preparatory work. International, governmental and non-governmental organizations liaising with the IEC also participate in this preparation. IEC collaborates closely with the International Organization for Standardization (ISO) in accordance with conditions determined by agreement between the two organizations.
2) The formal decisions or agreements of IEC on technical matters express, as nearly as possible, an international consensus of opinion on the relevant subjects since each technical committee has representation from all interested IEC National Committees.
3) IEC Publications have the form of recommendations for international use and are accepted by IEC National Committees in that sense. While all reasonable efforts are made to ensure that the technical content of IEC Publications is accurate, IEC cannot be held responsible for the way in which they are used or for any misinterpretation by any end user.
4) In order to promote international uniformity, IEC National Committees undertake to apply IEC Publications transparently to the maximum extent possible in their national and regional publications. Any divergence between any IEC Publication and the corresponding national or regional publication shall be clearly indicated in the latter.
5) IEC itself does not provide any attestation of conformity. Independent certification bodies provide conformity assessment services and, in some areas, access to IEC marks of conformity. IEC is not responsible for any services carried out by independent certification bodies.
6) All users should ensure that they have the latest edition of this publication.
7) No liability shall attach to IEC or its directors, employees, servants or agents including individual experts and members of its technical committees and IEC National Committees for any personal injury, property damage or other damage of any nature whatsoever, whether direct or indirect, or for costs (including legal fees) and expenses arising out of the publication, use of, or reliance upon, this IEC Publication or any other IEC Publications.
8) Attention is drawn to the Normative references cited in this publication. Use of the referenced publications is indispensable for the correct application of this publication.
9) IEC draws attention to the possibility that the implementation of this document may involve the use of (a) patent(s). IEC takes no position concerning the evidence, validity or applicability of any claimed patent rights in respect thereof. As of the date of publication of this document, IEC had not received notice of (a) patent(s), which may be required to implement this document. However, implementers are cautioned that this may not represent the latest information, which may be obtained from the patent database available at https://patents.iec.ch. IEC shall not be held responsible for identifying any or all such patent rights.

IEC TS 62607-9-2 has been prepared by IEC technical committee 113: Nanotechnology for electrotechnical products and systems. It is a Technical Specification.

The text of this Technical Specification is based on the following documents:

Draft	Report on voting
113/817/DTS	113/830/RVDTS

Full information on the voting for its approval can be found in the report on voting indicated in the above table.

The language used for the development of this Technical Specification is English.

This document was drafted in accordance with ISO/IEC Directives, Part 2, and developed in accordance with ISO/IEC Directives, Part 1 and ISO/IEC Directives, IEC Supplement, available at www.iec.ch/members_experts/refdocs. The main document types developed by IEC are described in greater detail at www.iec.ch/publications.

A list of all parts in the IEC 62607 series, published under the general title *Nanomanufacturing – Key control characteristics*, can be found on the IEC website.

The committee has decided that the contents of this document will remain unchanged until the stability date indicated on the IEC website under webstore.iec.ch in the data related to the specific document. At this date, the document will be

- reconfirmed,
- withdrawn, or
- revised.

IMPORTANT – The "colour inside" logo on the cover page of this document indicates that it contains colours which are considered to be useful for the correct understanding of its contents. Users should therefore print this document using a colour printer.

INTRODUCTION

Measurements of magnetic fields that are homogeneous over macroscopic volumes can be made traceable to the SI standards. Traceable calibration chains from national metrology institutes to the end users are well-established.

However, many important industrial applications rely on precision sensing of spatially varying magnetic fields. End-users need traceably quantitative characterization tools for magnetic materials on the micrometre to centimetre scale to perform quality management of their production processes.

IEC TS 62607-9-1 [1] [1] established high-resolution magnetic field measurements based on calibrated magnetic force microscopy. While qMFM can be regarded as the gold standard for nanoscale magnetic field measurements with highest spatial resolution, its technical application is often hindered by several drawbacks: qMFM does not provide a high time resolution and it has a limited scan range (typically up to 100 µm × 100 µm in commercial systems). Also, qMFM can only deal with samples that are flat on a 100 nm scale. On the other hand, nuclear magnetic resonance (NMR) based SI standards can only be applied to centimetre scale macroscopic objects. However, industrially relevant magnetic materials often combine micrometre scale magnetic features with sample dimensions in the millimetre or centimetre range and rough rather than flat surfaces.

Magneto-optical sensor technology is already used in the testing of magnetic materials and partly also for quality control of magnetic components. Prominent examples for such industrial samples with high economic relevance and high production numbers are:

– Magnetic scales for the fabrication of precise magnetic encoders for length measurement systems and rotary encoders, e.g. for automotive applications; relevant parameters to be metrologically assessed, like magnetic period, pole location, magnetic pole length, or pole width, are, for example, defined in the DIN SPEC 91411 [2].

– High-quality electrical steel sheets (grain-oriented SiFe alloys), which are used in rotating machinery and generators for efficient power generation and in transformers for low-loss electrical energy conversion. While the relevant metrological parameters are for example discussed in DIN EN 10107 [3], magneto-optical testing allows the magnetic and loss properties to be related to the underlying grain and domain structure.

This document closes the length scale gap for magnetic field measurements by establishing a quantitative magneto-optical indicator film measurement technique (qMOIF) for magnetic field distribution. qMOIF is a fast (sub second resolution) imaging technique, that allows a one-shot characterization of samples with areas of several square centimetres and with a resolution down to the micrometre range. It can be used under room temperature conditions and for direct sample testing without the need for costly and time-consuming surface treatments. qMOIF allows a near-field testing of the distribution of the stray magnetic field directly at the specimen surface. However, without magnetic and geometric calibration as well as proper adjustment of the setup geometry, qMOIF merely delivers qualitative stray field images. This results from the fact that the measured signal depends on the properties of magneto-optical indicator film used as well as on the setup geometry and the detector.

[1] Numbers in square brackets refer to the Bibliography.

MOIF imaging can be used in two basic operation modes that enable feature analysis and the characterization of quantitative stray field distributions, respectively.

a) The first mode, the “geometrical feature detection mode”, allows the characterization of the density and characteristic dimension of certain magnetic features on the basis of a magneto-optical image. The contrast is adjusted to give maximum contrast of certain features compared to the background. It is for example used for a dichotomization of the surface into areas with two distinct characteristics, like up and down magnetized domains. This mode is, for example, used for a quantitative characterization of domain widths and areal percentage.

b) The second mode, the “quantitative stray field distribution analysis mode”, allows one to perform a spatially resolved analysis of the stray field distribution above the surface of a sample. This demands a magnetic calibration that includes the characterization of the sensor and the setup. Thereby quantitative values of key control characteristics (KCCs) like magnetic field amplitudes are made accessible and ultimately become traceable to national calibration standards.

This document aims at providing a description of the measurement approaches for both above defined modes. This includes the adjustment of the setup and the traceable calibration and thus feature analysis as well as traceably calibrated field distribution measurements.

In summary, this document provides a traceable method for spatially resolved and quantitative micrometre-resolution measurements of magnetic field patterns with centimetre image sizes which can be applied to technologically relevant materials with flat surfaces. Thereby, it will further advance the precise control of fabrication processes and final product qualification. The values of the key control characteristics for those products are very product specific (see, for example, IEC TS 62622:2012 [4]).

NANOMANUFACTURING – KEY CONTROL CHARACTERISTICS –

Part 9-2: Nanomagnetic products – Magnetic field distribution: Magneto-optical indicator film technique

1 Scope

This part of IEC 62607 establishes a standardized method to determine the key control characteristic

- magnetic field distribution

of nanomagnetic materials, structures and devices by the

- magneto-optical indicator film technique.

The magnetic field distribution is derived by utilizing a magneto-optical indicator film, which is a thin film of magneto-optic material that is placed on the surface of an object exhibiting a spatially varying magnetic field distribution. The Faraday effect is then employed to measure the magnetic field strength by analysing the rotation of the polarization plane of light passing through the magneto-optic film.

– The method is applicable for measuring the stray field distribution of flat nanomagnetic materials, structures and devices.
– The method can especially be used to perform fast quantitative measurements of stray field distributions at the surface of an object.
– The magneto-optic indicator film technique is a fast, non-destructive method, making it an attractive option for materials analysis and testing in the industry.
– MOIF measurements can be done without any sample preparation and do not rely on specific surface properties of the object. It can be applied to the characterization of rough samples as well as of samples with non-magnetic cover layers.
– MOIF can quantitatively measure magnetic field distributions.
  - with a one-shot measurement which typically takes a few seconds
  - over areas of several square centimetres (over diameters of up to 15 cm with special techniques)
  - in a field range from 1 mT to more than 100 mT
  - with down to 1 µm spatial resolution
– Although techniques with nano-scale resolution are suitable for analysing the details of magnetic field structure, their ability to characterize larger areas is limited by their scanning area. Therefore, the MOIF technique is an indispensable complementary method that can offer a more comprehensive understanding of material properties.

This document focuses on the calibration procedures, calibrated measurement process, and evaluation of measurement uncertainty to ensure the traceability of quantitative magnetic field measurements obtained through the magneto-optic indicator film technique.

2 Normative references

There are no normative references in this document.

3 Terms and definitions

For the purposes of this document, the following terms and definitions apply.

ISO and IEC maintain terminology databases for use in standardization at the following addresses:

- IEC Electropedia: available at https://www.electropedia.org/
- ISO Online browsing platform: available at https://www.iso.org/obp

3.1 General terms

3.1.1
key control characteristic
KCC
key performance indicator
measurement process characteristic which can affect compliance with regulations and quality, reliability or subsequent application of the measurement result

Note 1 to entry: The measurement of a key control characteristic is described in a standardized measurement procedure with known accuracy and precision.

Note 2 to entry: It is possible to define more than one measurement method for a key control characteristic, if the correlation of the results is well-defined and known.

Note 3 to entry: In IATF 16949 the term "special characteristic" is used for a KCC. The term key control characteristic is preferred since it signals directly the relevance of the parameter for the quality of the final product.

3.2 General terms related to magnetic stray field characterization

3.2.1
magnetic-force microscopy
MFM
atomic force microscopy mode employing a probe assembly that monitors both atomic forces and magnetic interactions between the probe tip and a surface

[SOURCE: ISO 18115-2:2021, 3.1.15]

3.2.2
magneto-optical indicator film technique
MOIF technique
method of mapping the magnetic field above a sample surface by a thin magneto-optical Faraday-active indicator film

Note 1 to entry: The magnetic fields induce a declination of the magnetization from equilibrium direction in the active layer of the sensor, which is recorded with the Faraday effect.

3.3 Terms related to the measurement method described in this document

3.3.1
MOIF raw data distribution
$S(Nx, Ny)$, $S(x,y)$
pixel position, $S(Nx, Ny)$, for array sensors in wide field microscopes, or spatially resolved, $S(x,y)$, for sample scanning measurements in confocal microscopes, detector signal data array of a MOIF measurement

Note 1 to entry: The signal data type depends on the applied analysis technique. For direct MOIF measurements, raw data depict sensor dependent converted intensity distribution data in appropriate units. For differential, lock-in based MOIF measurements, raw data depict lock-in amplitudes in units of volt.

3.3.2
measurement height
h
value of the distance between the MOIF active layer surface facing the sample surface resulting from the sum of the measurement gap height g, the MOIF reflective coating thickness d^{rc} and the MOIF protective coating thickness d^{pc}

3.3.3
measurement plane
x-y-plane at the measurement height

Note 1 to entry: The MOIF measurement technique detects a signal which results from an averaging of field values over the sensor thickness. MOIF raw data therefore do not a priori represent the field distribution at the measurement height.

3.3.4
non-magnetic spacer
flat spacer of permeability $\mu = \mu_0$ placed in between the SUT and the sensor to adjust the measurement height

3.3.5
MOIF observation variable
raw data output of the detection unit

Note 1 to entry: The data type depends on the applied analysis technique. For direct MOIF measurements, raw data depict intensity distributions in appropriate units. For differential, lock-in based MOIF, raw data depict lock-in amplitudes in units of volt.

3.3.6
intensity detection unit
system to detect the light intensity distribution imaged by the imaging system after passing the polarizer

Note 1 to entry: The signal detection unit, typically a photo diode or an array sensor, converts light intensity into a digital signal.

3.3.7
z-scanner
element for the realization of the vertical displacement of the sample during x-y-scanning

Note 1 to entry: See ISO 18115-2:2021, 5.136

3.3.8
magnetic field reference sample
magnetic sample whose magnetic field distribution above the sample surface is well-known

3.3.9
image size
Sx, Sy
length and width of the sample area that is mapped into a two-dimensional raster image

3.3.10
pixel
smallest element of the digital image to which attributes are assigned

[SOURCE: ISO 10934:2020, 3.1.116]

3.3.11
pixel index
(Nx, Ny)
integer values indexing the position of a sensor unit in an array sensor

Note 1 to entry: These values also index the pixels of the mapped two-dimensional raster image.

3.3.12
pixel size
ΔA
sample area represented by each measured point in a two-dimensional raster image

$\Delta A = \Delta x \cdot \Delta y$

Note 1 to entry: The values for Δx and Δy are determined by the imaging geometry.

3.3.13
lateral position
(x, y)
coordinates in units of meters depicting the position on the sample under test

3.3.14
geometrical imaging function
function that describes in the case of a wide-field measurement geometry how a position on the sample (x, y) is mapped to the sensor pixels (Nx, Ny)

Note 1 to entry: The geometrical imaging function establishes an unambiguous and invertible relation between pixels and a set of discretized sample positions. In this sense, (x, y) and (Nx, Ny) can be used equivalently.

3.3.15
sample under test
SUT
material whose magnetic field distribution is to be measured

3.3.16
pseudo-Wiener deconvolution
deconvolution applying a pseudo-Wiener filter for noise suppression in a deconvolution in Fourier space with regularization parameter

Note 1 to entry: The formula that applies is as follows, where the asterisk marks the complex conjugate:

$$A(k,z) = \frac{B(k,z)}{C(k,z)} \quad \rightarrow \quad A(k,z) = B(k,z)\frac{C^{*}(k,z)}{\left|C(k,z)\right|^{2} + \mu}$$

3.3.17
regularization parameter
μ
constant in the *pseudo-Wiener deconvolution* (3.3.16) that approximates the noise characteristics of the image

3.3.18
transfer function
TF
two-dimensional arrays of complex data that represent operations on data that can be described by a convolution

3.3.19
field transfer function
TF^H
any transfer function that mediates an operation on magnetic field distributions and effective charge density distributions

Note 1 to entry: A field transfer function is used to calculate field distributions at heights different from the measurement plane.

3.3.20
discrimination
data treatment process where the data entries in a data distribution are dichotomized resulting in a binary data set with entries +1 or −1

Note 1 to entry: The dichotomization is effected on the basis of a threshold value t as discrimination criterion. Data entries less than t are assigned the value −1, data entries greater than or equal to t are assigned the value +1.

3.3.21
in-plane magnetic field
magnetic field vector with field components entirely in the measurement plane

3.3.22
out-of-plane magnetic field
magnetic field vector with field-components entirely perpendicular to the measurement plane

3.4 Terms related to the magneto optical indicator film (MOIF)

3.4.1
magneto-optical indicator film
MOIF
thin film magneto-optically active layer which is part of the MOIF sensor layer structure and which serves to detect magnetic fields exploiting the magneto-optical Faraday effect

Note 1 to entry: Typical MOIFs are based on ferrimagnetic bismuth-substituted rare-earth iron garnet, which are deposited on single-crystalline gadolinium gallium garnet (GGG) wafers by liquid phase epitaxy (LPE).

3.4.2
MOIF active layer
magneto-optically active MOIF volume

3.4.3
MOIF active layer thickness
d^{MOIF}
thickness of the magneto-optically active MOIF volume

3.4.4
MOIF type
anisotropy type of the MOIF, where "P" defines a planar (P-MOIF) with quality factor $Q < 1$ and "U" defines a uniaxial MOIF (U-MOIF) with $Q > 1$

3.4.5
MOIF reflective coating
reflective coating on the surface of the MOIF facing the sample

Note 1 to entry: MOIF reflective coating is typically a metallic coating or a dielectric mirror.

3.4.6
MOIF reflective coating thickness
d^{rc}
thickness of the MOIF reflective coating

3.4.7
MOIF protective coating
protective coating on the surface of the MOIF sensor that faces the sample, typically an oxide coating or a hard coating

3.4.8
MOIF protective coating thickness
d^{pc}
thickness of the MOIF protective coating

3.4.9
MOIF magnetic anisotropy constant
constant that describes the magneto-crystalline anisotropy and thus the dependency of the material's free energy on the orientation of the magnetization

Note 1 to entry: K_{uoop}, K_{uip}, K_{c} represent the out-of-plane (oop), in-plane (ip) and cubic anisotropy contributions, respectively.

3.4.10
MOIF magnetic anisotropy field
effective field that describes the material's magnetic anisotropy and thus the dependency of the material's free energy on the orientation of the magnetization

Note 1 to entry: B_{uoop}, B_{uip} *and* B_{c} represent the out-of-plane (oop), in-plane (ip) and cubic anisotropy contributions, respectively.

Note 2 to entry: Anisotropy constants and anisotropy fields are related via:

$$K_{\mathrm{ani}} = B_{\mathrm{ani}} \cdot M_{\mathrm{S,MOIF}} / 2$$

3.4.11
MOIF saturation magnetization
$M_{\mathrm{S,MOIF}}$
saturation magnetization of the MOIF active layer in perpendicular direction

Note 1 to entry: $M_{\mathrm{S,MOIF}}$ typically is MOIF temperature dependent, $M_{\mathrm{S,MOIF}}(\mathrm{T})$ and thus needs to be given for the MOIF temperature T_{sensor} during the measurement.

3.4.12
MOIF magnetization vector
magnetization vector of the MOIF active layer either as a vector or in the form of the vector's cartesian or cylindrical coordinates

Note 1 to entry: The MOIF magnetization vector can be described as $\vec{M}$ or by its cartesian coordinates M_{x}, M_{y} and M_{z} or its cylindrical coordinates (M, θ^{M} and φ^{M}), which give the magnitude and the polar and azimuthal angle of the magnetization vector, respectively, in a coordinate system with the polar direction perpendicular to the MOIF surface.

3.4.13
MOIF normalized magnetization vector
normalized magnetization vector of the MOIF active layer $\vec{\hat{M}} = \frac{\vec{M}}{|M|}$, either as a vector or in the form of the vector's cartesian or cylindrical coordinates

Note 1 to entry: The MOIF normalized magnetization vector can be described as $\vec{\hat{M}}$ or by its cartesian coordinates $\hat{M}_{\mathrm{x}}$, $\hat{M}_{\mathrm{y}}$ and $\hat{M}_{\mathrm{z}}$ or its cylindrical coordinates ($\hat{M}$, θ^{M} and φ^{M}), which give the magnitude and the polar and azimuthal angle of the normalize magnetization vector, respectively, in a coordinate system with the polar direction perpendicular to the MOIF surface.

3.4.14
saturation
<of the MOIF sensor> situation where the MOIF magnetization is aligned perpendicular, i.e. $\hat{M}_x = 0$, $\hat{M}_y = 0$, $\hat{M}_z = 1$

Note 1 to entry: It is possible that the saturation is only reached asymptotically. This requires a definition of a cut-off criterion for $\hat{M}_z$.

3.4.15
saturation field strength
H_z^{sat}
perpendicular magnetic field for which the MOIF reaches saturation

Note 1 to entry: Saturation field strength defines the operating range of the MOIF sensor where a calibration can be performed.

Note 2 to entry: It is possible that saturation is only reached asymptotically. H_z^{sat} then has to be chosen in a meaningful way, e.g. as the H_z value where the interpolated linear part of the $M_z(H_z)$ curve reaches M_z = 1.

3.4.16
MOIF quality factor
Q
parameter characterizing ferromagnetic thin films with an easy axis of magnetization normal to the film plane

$$Q = 2K_{uoop} / \mu_0 M_S^2,$$

where K_{uoop} is the uniaxial anisotropy constant.

Note 1 to entry: Q defines the ratio between the energy of magneto-crystalline anisotropy and maximum energy density due to shape anisotropy. For Q > 1, the film will be uniaxial with out-of-plane easy direction, while for Q < 1, the magnetic moments will tend to be oriented in the plane of the film due to shape anisotropy.

3.4.17
MOIF figure of merit
FOM
value that describes the merit of a MOIF by comparing Faraday effect amplitude and optical absorption

Note 1 to entry: A high value of the FOM is required for imaging a wide spectrum of object feature sizes.

Note 2 to entry: The MOIF figure of merit is calculated from the optical absorption, γ, and the Faraday rotation in saturation, α_{sat} as $FOM = 2\alpha_{sat} / \gamma$.

3.4.18
Verdet constant
v
parameter of the MOIF material that quantifies the Faraday effect strength at a particular wavelength of light

Note 1 to entry: v is a function of the material and of the wavelength: $v = v(\omega)$.

Note 2 to entry: The Faraday rotation linearly depends on the Verdet constant, the length of the path of the light through the optically active medium and the perpendicular magnetization component M_z of the optically active medium. For MOIF measurements, the Faraday rotation in reflection is given by:

$$\alpha = 2\, d^{MOIF}\, v(\omega)\, M_z.$$

3.5 Terms related to Faraday rotation

3.5.1
Faraday rotation
α
angle of rotation of the plane of polarization of the light passing the MOIF sensor due to the local perpendicular magnetization component M_z of the sensor

Note 1 to entry: The Faraday rotation is also wavelength dependent and increases with decreasing wavelength. The typical absorption band below 530 nm results in increased Faraday ellipticity. Thus, the typical wavelength range in the application is between 530 nm and 630 nm, depending on the properties of the MOIF. Monochromatic light can be used, but also white light.

3.5.2
Malus law
law that gives the intensity I of polarized light after passing a polarizer at an angle θ

$$I = I_0 \cos^2(\theta)$$

3.5.3
absorption coefficient
γ
wavelength-dependent material parameter that determines how far light of a particular wavelength can penetrate into the material before it is absorbed

3.5.4
effective anisotropy field
B_A
effective perpendicular anisotropy field of the MOIF active layer that results from the interaction of crystalline anisotropy contributions and the demagnetization field

3.5.5
demagnetization field
B_{demag}
effective field caused by the sample magnetization due the sample shape that describes the tendency to reduce the total magnetic moment of the specimen

Note 1 to entry: The demagnetization field is quantified by the demagnetization tensor.

3.5.6
MOIF transfer function
TF^{MOIF}
transfer function for calculating the real field distribution at the surface of the sensor that faces the sample from the measured raw field distribution by accounting for the averaging over the MOIF's finite active layer thickness

3.5.7
MOIF flatness parameter
parameter that describes the waviness of the MOIF

EXAMPLES mean depth of waviness motifs (W), mean spacing of waviness motifs (AW), maximum depth of waviness motifs (Wx) and amplitude of the upper envelope (Wte)

3.5.8
MOIF nominal surface plane
mathematically defined plane that defines the surface of the active layer that faces the sample surface during measurements as specified by the design

3.5.9
MOIF roughness parameter
parameter that describes the roughness of the MOIF surface

EXAMPLES mean depth of roughness motifs (R), mean spacing of roughness motifs (Ar) and maximum depth of roughness motifs (Rx)

3.6 Terms related to the magneto-optical measurement setup

3.6.1
magneto-optical measurement setup
entirety of the light source, optical system, MOIF itself and detection unit, possibly with magnetization unit to apply magnetic fields to the sample

3.6.2
optical system
entirety of the optical devices forming the optical path, including light source, analyser, polarizer, beam splitter, Faraday rotator, objective and lenses, if applicable

3.6.3
light ray
light traveling in any direction in a straight line

3.6.4
light beam
bundle of light rays

3.6.5
wide field imaging geometry
measurement geometry where the entire sample is exposed to light and the sample is imaged to an array sensor

3.6.6
spot measurements
measurement technique where only one spot on the sample is exposed to light and light reflected from the spot is detected by a sensor

3.6.7
measurement gap
g
distance between the surface of the MOIF sensor facing the sample and the sample surface

Note 1 to entry: The surface of the MOIF sensor facing the sample can be the surface of the MOIF reflective coating or the MOIF protective coating or, if no coating is used, the surface of the active layer.

3.6.8
angle of rotation of the plane of polarization
β
angle of rotation of the polarized light in the reflected light beam after passing the MOIF twice relative to the plane of polarization of the incoming light

3.6.9
light source
optical device to create light with a defined optical spectrum, typically an LED or LED array, an arc source or a laser which can be combined with bandpass filters

3.6.10
intensity
I
general term for the strength of a radiation which is proportional to the square of the amplitude of the electromagnetic wave

[SOURCE: ISO 10934:2020, 3.1.79]

3.6.11
filter
optical device designed to control selectively the wavelengths, colour temperature, vibration direction, and/or intensity of the radiation which it transmits or reflects

[SOURCE: ISO 10934:2020, 3.1.55]

3.6.12
radiation
energy in the form of electromagnetic waves or particles

[SOURCE: ISO 10934:2020, 3.1.123]

3.6.13
light
electromagnetic radiation directly capable of causing a visual sensation

[SOURCE: ISO 10934:2020, 3.1.88]

3.6.14
polarizing filter
filter (3.6.11) acting as a polar (ISO 10934:2020, 3.1.118) by total or partial absorption of *light* (3.6.13) vibrating in certain directions

[SOURCE: ISO 10934:2020, 3.1.55.12]

3.6.15
polarizer
polarizing filter that is used to filter light in such a way that only linearly polarized light in a given orientation is transmitted

Note 1 to entry: In the optical path, it is placed after the light source and before the optically active medium (MOIF).

3.6.16
analyser
device that has the same functionality as the *polarizer* (3.6.15) but is used to analyse the orientation of the polarization plane of the light by converting it to an intensity contrast

Note 1 to entry: In the optical path, it is placed after the polarizer and the optically active medium (MOIF) before the intensity detection unit.

3.6.17
analyser operating angle
θ
clockwise deviation of the angle of the analyser from the crossed position of polarizer and analyser when looking in the direction of propagation of the beam

3.6.18
beam splitter
optical device that is used to split an incoming light beam into two separate light beams which can have different intensities

Note 1 to entry: In magneto-optical setups with normal or near normal incidence of the incident light beam, a beam splitter can be used to separate the beam paths of incoming light and the light reflected from the sensor. The reflected light is thereby deflected to the detection unit.

Note 2 to entry: Typically, the ratio of reflection and transmission is 50/50 at an angle of incidence of 45°.

3.6.19
Faraday rotator
optical device that induces a certain rotation of the polarization plane of polarized light

Note 1 to entry: In MOIF measurements, this adds to the polarization rotation of the light beam reflected from the MOIF sensor which is caused by the MOIF magnetization M_z.

3.6.20
Faraday modulator
adjustable Faraday rotator that induces a small periodic deviation of the light polarization

Note 1 to entry: In MOIF measurements, this periodic deviation of the light polarization adds to the rotation of the polarization plane of the light reflected from the MOIF reflective coating before passing the analyser. In combination with lock-in detection this works as an analogue differentiator for the light intensity.

3.7 Terms related to optical microscopy

3.7.1
objective
component that is used is used in optical microscopy to enhance the lateral resolution in x and y

3.7.2
imaging optics
part of the optical system that images or projects the object plane on the detection unit

Note 1 to entry: In MOIF measurements, the measurement plane at the measurement height is mapped to the detection unit.

3.7.3
microscope
instrument designed to extend visual capability, i.e. to make visible minute detail that is not seen with the unaided eye

[SOURCE: ISO 10934:2020, 3.1.99, modified – Note 1 to entry has been deleted.]

3.7.4
scanning optical microscope
microscope specially designed to scan the object plane in a raster pattern

Note 1 to entry: There are two techniques of scanning: one is based on movement of the illuminating beam with the object remaining stationary, the other on the movement of the object, the beam remaining stationary. The instrument can be operated in the confocal imaging mode.

[SOURCE: ISO 10934:2020, 3.1.99.12 modified – In the definition, "or image plane" has been deleted. The first sentence of Note 1 to entry has been deleted.]

3.7.5
MOIF setup
entirety of the MOIF system including light source, optical system, magneto-optical sensor and detection unit, possibly with magnetization unit to apply magnetic fields to the sample

3.8 Terms related to the setup calibration process

3.8.1
sensor signal
S, $S(Nx, Ny)$
signal of a sensor in an appropriate representation

Note 1 to entry: As an example, an appropriate representation is volt for a photodiode and a 12-bit integer for a CCD or CMOS chip.

Note 2 to entry: For array sensors, S is a distribution of signal values over the pixel indices i and j, $S(i, j)$.

3.8.2
sensor sensitivity function
$s(I)$, $s(Nx, Ny, I)$
function that relates the light intensity of the light at the position of the sensor to the measured signal, $S = s(I)$

Note 1 to entry: For array sensors, s is a function of the pixel indices (i,j), and thus $S(i, j) = s(i, j, I)$. Sensors are linear if the relation between signal and intensity can be described by a relation

$$S = C \cdot I, \text{ and thus } s(I) = C \cdot I$$

with a constant factor C.

3.8.3
light intensity at the detection unit
I^{det}, $I^{det}(Nx, Ny)$
light intensity at the position of the intensity detection unit

Note 1 to entry: For array sensors, I^{det} is a function of the pixel indices (Nx, Ny), and thus $I^{det}(Nx, Ny)$.

3.8.4
intensity of the incident polarized light beam at the sensor position
I^{inc}, I^{inc} (x, y)
light intensity of the incident light in the measurement plane

Note 1 to entry: For array sensors, I^{inc} is a function of the position on the sample (x, y), and thus $I^{inc}(x, y)$.

3.8.5
reflected light intensity
I^{refl}, I^{refl} (x, y)
parameter that describes the intensity of the light reflected from the sensor in the measurement plane

Note 1 to entry: For wide-field images, I^{refl} is a function of the position on the sample (x,y), and thus $I^{refl}(x, y)$.

3.8.6
MOIF calibration array in out-of-plane magnetic fields
$F^{cal}(Nx, Ny)$
experimentally determined dataset of the signal S detected by the detection system in appropriate units as a function of the applied out-of-plane external field H_z and of the pixel indices (Nx, Ny)

Note 1 to entry: The data may be collected on only a (representative) subset of the sensor pixels. For each pixel, $F^{cal}(Nx, Ny)$ is given as an array for discrete values of $H_z(Nx, Ny)$ versus $S(Nx, Ny)$.

3.8.7
MOIF calibration curve in out-of-plane magnetic fields
$F^{cal,fit}(Nx, Ny)$
parametrized fit to the $F^{cal}(Nx, Ny)$ or rules for numerical interpolation of the $F^{cal}(Nx, Ny)$, data that allows one to relate a measured signal S to a unique H_z value (with sign) for each pixel (Nx, Ny)

3.8.8
setup calibration range
field range for which the calibration is valid

3.9 Terms related to the magneto-optical measurement process

3.9.1
lateral resolution in x and y
$\Delta x, \Delta y$
minimum distance at which two distinct magnetic features of a specimen are distinguishable

Note 1 to entry: The lateral resolution depends on the optical system, the pixel size of the detection unit and on the properties of the MOIF.

3.9.2
magnification
process of changing the apparent dimensions of an object by optical techniques

[SOURCE: ISO 10934:2020, 3.1.90, modified – ", or the numerical expression of the result of this" has been deleted from the end of the definition. The Notes to entry have been deleted.]

3.9.3
image
representation of the MOIF measurement raw data, corresponding to points in the sample

3.10 Key control characteristics measured according to this standard

3.10.1
data acquisition time
t
time period over which the detection unit integrates the intensity of the incoming light

3.10.2
frame averaging
averaging the pixel values from sequential images recorded under identical conditions.

Note 1 to entry: Used to increase signal-to-noise ratio.

[SOURCE: ISO 10934:2020, 3.2.22, modified – In the definition, "digital or electronic images" has been replaced with "images".]

3.10.3
number of averages
N
parameter that describes how many times the single imaging process was repeated for the calculation of the final averaged image to enhance signal to-noise ratio

3.10.4
sensor calibration temperature
$T^{\text{cal,sensor}}$
temperature of the sensor during the calibration

Note 1 to entry: The temperature must not be identical with the environmental temperature during calibration since the sensor is heated by the illuminating light.

3.10.5
environmental calibration temperature
$T^{\text{cal,env}}$
temperature of the environment during calibration

3.10.6
sensor measurement temperature
T^{sensor}
temperature of the sensor during the measurement

Note 1 to entry: The temperature must not be identical with the environmental temperature during calibration since the sensor is heated by the illuminating light.

3.10.7
environmental measurement temperature
T^{env}
temperature of the environment during the measurement

3.10.8
magnetic field distribution
H_z
spatially resolved magnetic field data array of the perpendicular magnetic field component measured in the x-y-plane with the x-, y-direction in the sample plane and the z-direction along the sample surface normal with a spatial resolution dx, dy at a distance d above the surface of a test sample

EXAMPLE The magnetic field distribution of a sample under test is called H_z^{SUT}.

4 Symbols and abbreviated terms

Abbreviated terms and symbols are given in Table 3 and Table 4, respectively.

Table 1 – Abbreviated terms

Abbreviated term	Description
DFT	discrete Fourier transform
FOM	figure of merit
ip	in-plane
KCC	key control characteristic
MOIF	magneto-optical indicator film
oop	out-of-plane
qMOIF	quantitative magneto-optical indicator film technique
SUT	sample under test
TF	transfer function

Table 2 – Symbols

Symbol	Corresponding uncertainty (if applicable)	Description
μ	$u\mu$	regularization parameter
$S^{SUT}(x,y)$, $S^{SUT}(k)$	uS^{SUT}	reference sample measurement raw data (detection unit signal) in real, partial Fourier space
$\Delta A = \Delta x \times \Delta y$	$u\Delta A$, $u\Delta x$, $u\Delta x$	pixel size in x-direction, y-direction
RH		Environmental relative humidity
$H_z^{SUT}(x,y,z)$, $H_z^{SUT}(k,z)$	uH_z^{SUT}	z-component of the magnetic field distribution of the SUT in real, partial Fourier space
k_x, k_y		spatial wave vector components in x-direction, y-direction in partial Fourier space
$k = (k_x, k_y)$		vector of the spatial wave vectors in x-direction, y-direction in partial Fourier space
$k = \sqrt{k_x^{\,2} + k_y^{\,2}}$		modulus of the vector of the spatial wave vectors
K_u, K_d		perpendicular MOIF magnetic anisotropy constant, magneto-static energy density
$m(x,y)$, $m(k_x, k_y)$		normalized magnetization distribution in real / Fourier space
M_S	uM_S	MOIF saturation magnetization
Nx, Ny		pixel number in x-direction, y-direction
Q	uQ	MOIF quality factor
Sx, Sy		image size in x-direction, y-direction
T^{env}	uT	environmental measurement temperature
θ	uθ	rotation angle of the analyser relative to a crossed position of analyser and polarizer
s		sensor sensitivity function
x,y	ux, uy	in-plane scan spatial coordinates
h	uh	measurement height
g	ug	measurement gap

5 General

5.1 Measurement principle

5.1.1 Overview

The MOIF microscopy as described in this document detects and measures magnetic stray field distributions using an optical microscopy technique employing a reusable magneto-optical (MO) indicator film that is placed on top of the sample under test. A comprehensive review on MOIF can be found in [5].

The optically transparent indicator film is illuminated by polarized light (visible range) from the back side and the light is reflected from the mirrored sensor film side, thereby passing the sensor thickness twice, while transmitted through the sensor the light undergoes a high Faraday rotation proportional to the local stray field and the sensor thickness. Consequently, the observed polar Faraday rotation is a measure for the normal component of the sample stray field. In contrast to Magneto-Optical Kerr Effect (MOKE) microscopy, MOIF microscopy works independently of the optical properties of the sample and does not require optically smooth surfaces or samples with intrinsic high effect amplitudes. Plane surfaces of magnetic components can be characterized two-dimensionally in direct contact to the sensor in a one-shot measurement.

MOIFs were first used for qualitative studies of low temperature superconductors with the aid of phosphate glasses and films of EuS, EuF2, and EuSe which were deposited directly on the superconductor samples resulting in a resolution close to the optical diffraction limit [6], [7]. Unlike MOIFs deposited directly onto the sample, free standing, freely movable MOIF sensors can be used for non-destructive characterization. For this purpose, high-quality single-crystalline ferrite garnet films were grown by the method of liquid phase epitaxy (LPE) [5], typically on gadolinium gallium garnet substrates (GGG). Micrometre-thick iron garnet films deposited with different LPE parameters show different magnetic properties and can be classified by their anisotropy in perpendicular [8], [9], [10], [11], [12], [13], [14] or in-plane [15], [16], [17], [18] MOIF. Disposable MOIF sensors were initially introduced for the characterization of current distributions [18], [19], [20] and individual Abrikosov vortices [21] in high-temperature superconductors. Reviews on magneto-optical investigations on superconductors can be found in [20], [22]. The possibility to analyse current distribution via their related magnetic field distribution was further exploited for the analysis of eddy current distributions [23], [24], [25], [26] and currents in integrated circuits [27].

Ferrimagnetic bismuth-substituted iron garnet films with enhanced Faraday rotation can be deposited on a 15-cm wafer scale and thus with chip sizes of several square centimetres [28]. That allows large sample areas to be characterized [29]. One shot measurement of large area samples combined with short data acquisition times allows imaging of dynamic processes [30], [31], [32] on a kilohertz frequency range. Since MOIF detects stray fields, they can be applied to the characterization of hidden structures and non-flat samples [33].

The mirrored sensor side can be protected with a low-friction hard coating that allows the sensor to be brought in direct mechanical contact with the specimen during the measurement and thus in the near field of the sample surface. By that, a spatial resolution down to below 1 µm can be achieved. Magneto-optical systems using in-plane magnetized MOIF sensors can be calibrated to quantitatively determine magnetic field strengths in the range of 0,05 kA/m to 100 kA/m after a once-in-a-lifetime calibration process. The properties of indicator films can be tailored to fit the respective measurement needs with respect to sensitivity and field amplitude and can be optimized to yield a high effect amplitude and thus a high signal-to-noise ratio. Nowadays, large MOIF sensor chips combined with digital camera technology allow a simultaneous detection of stray fields up to several square centimetres without the need for scanning.

5.1.2 Magneto-optical indicator films

5.1.2.1 Chemistry

MOIFs are typically single-crystalline ferrite garnet films. Ferrite garnets $\{R^{3+}{}_3\}[Fe^{3+}{}_2](Fe^{3+}{}_3)O_{12}$ have a cubic structure with rare earth and iron ions occupying different positions ({R} dodecahedral, [Fe] octahedral and (Fe) tetrahedral) between oxygen ions.

5.1.2.2 Fabrication

MOIF are grown by liquid phase epitaxy (LPE) from high temperature solutions on substrates like gadolinium gallium garnets (GGG).

5.1.2.3 Magnetic properties

This document focuses on in-plane MOIF films (P-MOIF). A typical magnetization curve of an in-plane MOIF is shown in Figure 1.

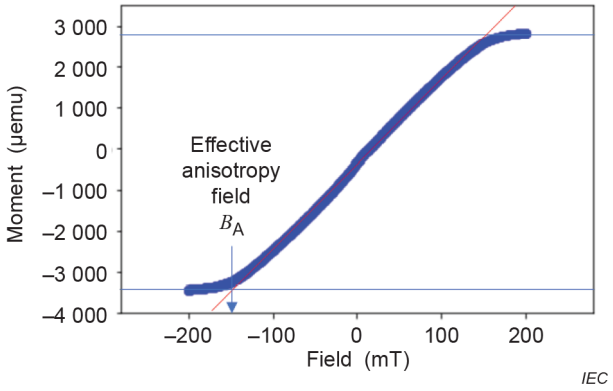

Figure 1 – Typical MOIF hysteresis curve and effective MOIF anisotropy field B_A

The magnetization curve of an ideal MOIF is hysteresis free. The example in Figure 1 shows some deviations from linearity and the process of how to geometrically determine the effective anisotropy field from an interpolation of the measured curve.

5.1.3 Sensor

5.1.3.1 General

The layer sequence of a typical MOIF sensor is shown in Figure 2. The magneto-optical indicator film is an assembly of up to three layers: a magneto-optically active layer, a reflective layer and a protective layer. See, for example, [5] and [37],

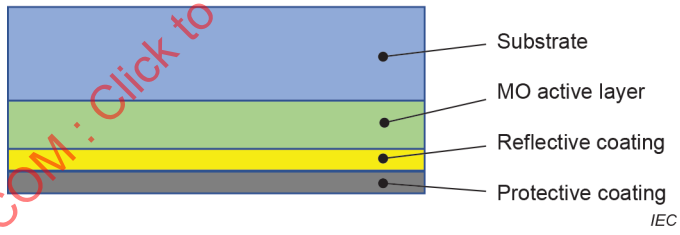

Figure 2 – Schematic of the functional layers of a MOIF sensor

5.1.3.2 Substrate

The substrate supports the active layer and provides the crystallographic orientation and lattice constant for epitaxial film growth. It is optically transparent, paramagnetic and has a negligible, very low Verdet constant. Due to its film thickness in the micrometre range and very high Verdet constant, the MOIF dominates the Faraday rotation of the sensor.

5.1.3.3 Magneto-optical indicator film (active layer)

The active sensing layer is a magneto-optically active single-crystalline garnet film that is predominantly transparent in the range of visible light (VIS), and that has a large specific Faraday rotation and high magneto-optical sensitivity. The MOIF has a typical thickness d^{MOIF} between 0,5 µm and 5 µm. Thinner sensors show a low absolute Faraday rotation, but a better spatial lateral resolution in x and y.

The lower Faraday rotation can reduce the signal-to-noise ratio of the sensor.

MOIFs have a defined specification with tight tolerances in terms of absorption, defined film thickness, absolute Faraday rotation, saturation field strength and defect sizes. The different magneto-optical characteristics of each sensor type, due to magnetic compensation and anisotropy, are optimized for room temperature applications, High reproducibility of sensory properties, a high level of control in the manufacturing process and quality control ensure the use of adequate magneto-optical sensors in stray field imaging systems.

5.1.3.4 MOIF reflective coating

The light from the light source is transmitted through the active layer and passes the active layer a second time after being mirrored at the reflective layer.

Ideally, the mirror system has a very good adhesion to the MOIF surface, high optical reflectivity (typically greater than 99 %) for light wavelengths in the VIS, and sufficiently high mechanical stability.

5.1.3.5 MOIF protective coating

The protective layer is a hard coating that protects the reflective layer from being scratched when brought in close contact with the sample. This adequate hard material ensures high mechanical wear resistance during use in systems. In addition to high hardness, the wear protection material has high adhesion to the mirror surface, low friction coefficient and optical absorption of VIS wavelengths.

5.1.4 Faraday effect in reflection

The Faraday effect describes the rotation of the polarization plane of linearly polarized light when traversing the magneto-optical sensor film. Working in reflection doubles the Faraday effect, allowing back illumination from the GGG side and enables direct positioning of the specimen to the front of the magneto-optical sensor. The local Faraday rotation in the sensor plane is caused by the local magnetization of the MOIF which is induced by the spatially varying magnetic stray field of the sample.

5.1.5 Measurement scheme

The measurement scheme for quantitative stray field distribution analysis is depicted in Figure 3. The sample is positioned with its surface in close contact to the MOIF protective coating (mirrored MOIF side). The sample stray field magnetizes the active layer. The polarized light from a light-source passes through the active layer, is reflected at the reflective layer and then passes the active layer a second time. The polarization plane of the light is rotated due to the Faraday effect. The amplitude of the Faraday effects depends on the local orientation of the sensor magnetization. The angle of rotation of the plane of polarization is translated into a measurement signal by the detection unit. Low-hysteresis in-plane MOIFs (very low remanence and coercivity) exhibit pure domain rotation in the dynamic range.

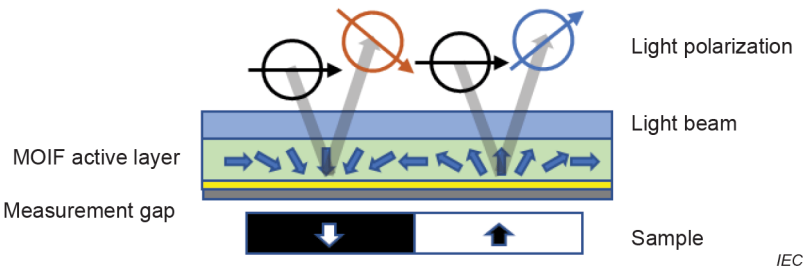

Figure 3 – Schematic MOIF setup

5.1.6 MOIF signal generation theory

The incident beam path and the passage through the sensor are not dependent on the MOIF detection scheme. The following discussion is limited to planar P-MOIF sensors with pure in-plane anisotropy, and thus $K_{uoop} < 1$. Additionally, pure out-of-plane fields, $H = (0,0,H_z)$ are assumed. The discussion closely follows the discussion in Jooss et al. [20]. The reflected light intensity I^{refl} with sensor thickness d^{MOIF} and absorption coefficient γ is given by

$$I^{refl} = I^{inc} e^{-2\gamma d^{MOIF}} \tag{1}$$

where I^{inc} represents the intensity of the incident polarized light beam at the sensor position.

Additionally, the reflected light undergoes a Faraday rotation α directly proportional to the perpendicular magnetization component M_z of the sensor.

$$\alpha = 2 d^{MOIF} v(\omega) M_z \tag{2}$$

where $v(\omega)$ is the light frequency ω dependent Verdet constant.

For $Q < 0$ and purely oop fields H_z the relation between M_z and H_z is given by (see A.3.1)

$$M_z = M_{S,MOIF} \cos(\theta) = M_{S,MOIF} \frac{H_z}{H_A}, \tag{3}$$

Where H_A is an effective anisotropy field $H_A' = H_A + M_{S,MOIF}$. H_A is the anisotropy field resulting from the magneto-crystalline energy contribution. H_A' additionally accounts for the demagnetization field of the canted MOIF magnetization vector. The relation between the Faraday rotation α and H_z can thus be found as

$$\alpha = 2 d^{MOIF} v(\omega) M_z = 2 d^{MOIF} v(\omega) M_{S,MOIF} \frac{H_z}{H_A}, \tag{4}$$

The influence of additional in-plane magnetic field components is discussed below.

5.1.7 MOIF measurement modes

Based on the imaging process described above, two principal measurement modes can be realized and are discussed here:

a) geometrical feature detection mode;

b) quantitative spatially resolved stray field analysis mode.

5.1.8 Feature detection mode

In the feature detection mode, sensors with either out-of-plane, MOIF type U, or in-plane , MOIF type P, magnetic anisotropy are used. Sensors with out-of-plane anisotropy exhibit a meander domain structure. They allow to detect fields well below 1 mT and thus can be applied to low stray field materials like grain-oriented steel sheets. In these sensors, perpendicular magnetic fields lead to a growth of domains aligned with the field at the expense of domains with the opposite orientation (domain wall displacement). This induces a change in the average MOIF signal (averaged over several of the micrometre-scale domains) and thus to a field dependent contrast. Due to the meander domains and their domain width up to 10 µm, the lateral resolution in x and y of the stray field imaging within the sensor is limited.

5.1.9 Quantitative spatially resolved feature detection mode

Quantitative spatially resolved stray field analysis is done with MOIF sensors with in-plane anisotropy, MOIF type P, and can be applied to quantitatively detect magnetic field in a typical range of 0,05 kA/m to 100 kA/m. Quantitative determination of local field strengths requires low-hysteresis in-plane sensors that exhibit predominantly domain rotation depending on the stray field. The domain rotation is cleanly reversible and thus always allows a uniquely discrete relation between the local Faraday rotation and the local magnetic field of the sample. The lateral resolution in x and y is determined by the detecting optical system, the MOIF thickness, and the distance to the sample. The quantitative spatially resolved stray field analysis mode requires a calibration of the MOIF raw signal. Additionally, it is required to quantify the influence of in-plane magnetic field components.

5.2 Description of measurement equipment or apparatus

5.2.1 MOIF imaging system

The imaging system serves to create a spatially resolved representation of the reflected light beam (relative to incident light beam) at the plane of the MOIF nominal surface plane that is turned away from the sample. The spatially resolved light signal from the MOIF sensor is then detected by a detection unit that can either comprise a single sensor [34] or an array sensor [37]. The two most common imaging schemes are confocal imaging in a scanning optical microscope and wide field imaging geometry, see Figure 4 a) and b). Figure 4 only shows the path of the light, all aspects related to polarization and detection are discussed in 5.2.4. In an inverted scheme, the geometry is rotated by 180° so that the sample can be laid onto the sensor instead of putting the sensor onto the sample.

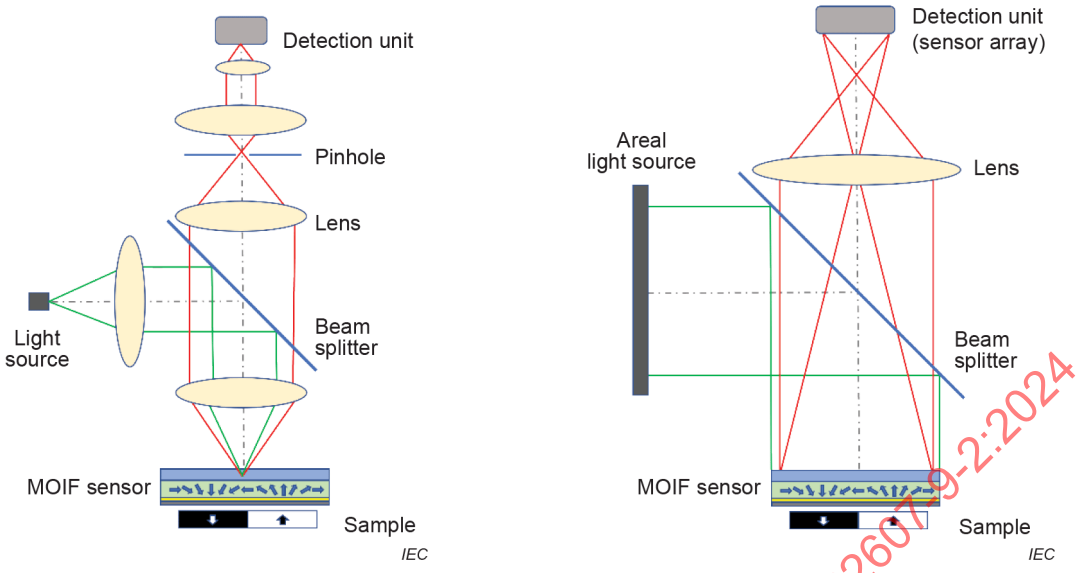

a) spot geometry **b) wide field imaging geometry**

NOTE In an inverted scheme, the geometry is rotated by 180° so that the sample can be laid onto the sensor instead of putting the sensor onto the sample.

Figure 4 – Imaging geometries that can be used for MOIF imaging

5.2.2 MOIF imaging systems for spot measurements, confocal microscopy

In MOIF spot measurements (Figure 4 a), the incident beam is focused into a (diffraction limited) spot on the measurement plane, typically by an objective in a confocal microscope geometry. The reflected light then passes the focusing optics a second time, passes the beam splitter and is then detected by a single non spatially resolving detection unit. For the detection by the detection unit, additional optical imaging can be required. Spatially resolved two-dimensional images of the measurement plane are achieved by scanning either the sample or the light spot.

5.2.3 Imaging systems in wide field geometry

In wide field imaging geometry (Figure 4 b), the measurement plane is mapped onto an array sensor. The signal distribution measured by the sensor array therefore reflects a spatially resolved discretized representation of the magnetization stray field distribution at the measurement height.

The geometrical imaging function establishes an unambiguous and invertible relation between pixels and a set of discretized sample positions. In this sense, (x, y), referring to a position on the sample, and (Nx, Ny), referring to a position on the array sensor, can be used equivalently. Correspondingly, the sample position data (x, y) are either representing discrete or continuous position data as supported by the context.

5.2.4 MOIF signal detection

The MOIF signal generated by the detection unit is a measure of the (spatially varying) angle of rotation of the polarization plane of the incident polarized light beam. It is converted into an electrical signal which then is protocolled as the measurement signal. In this document three conversion approaches are discussed: a technique employing a polarization filter as an analyser [37], a “differential” detection approach which uses an additional Faraday modulator [34], and a quantitative direct polarization measurement technique using a polarization camera [35].

5.2.5 MOIF signal detection schemes overview

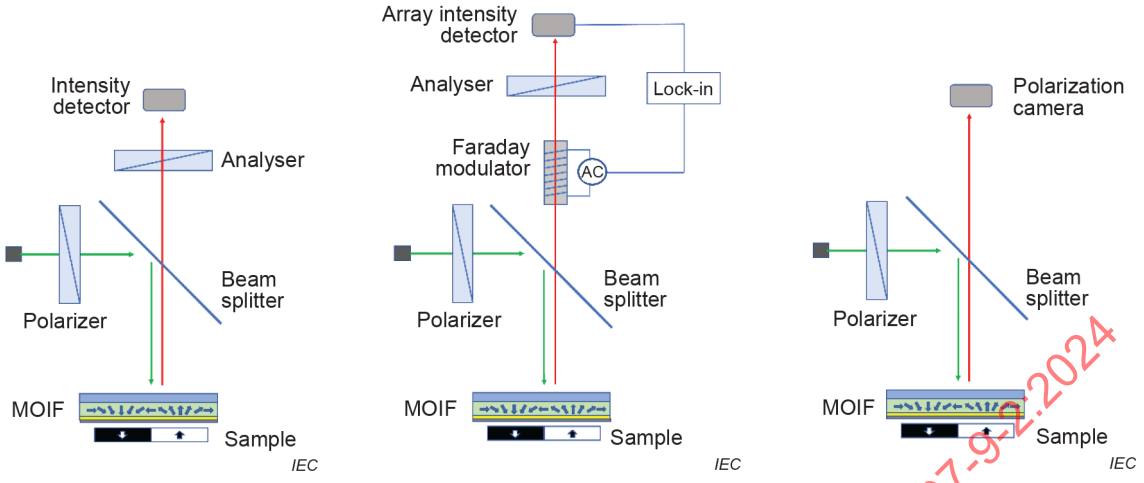

a) analyser based **b) analyser-based differential** **c) polarization camera-based**

Figure 5 – MOIF measurement schemes for detection of the Faraday rotation

5.2.6 MOIF signal detection by a polarizing filter as an analyser

The measurement scheme for MOIF measurements using an analyser is shown in Figure 5 a).

The light is generated by a light source. After passing the polarizer, the incident light passes the sensor substrate and the MOIF, is reflected by the sensor reflecting layer and then passes the active layer a second time. The reflected light beam shows a Faraday rotation proportional to the local sensor magnetization M_z. When the reflected light beam passes the analyser, the Faraday rotation is converted into an intensity contrast which is detected by an intensity detection unit.

5.2.7 Differential MOIF signal detection by a polarizing filter plus a Faraday rotator to modulate the signal for lock-in detection

The measurement scheme for differential MOIF measurements is shown in Figure 5 b).

Compared to the approach discussed in 5.2.6, here a Faraday modulator is added which allows a periodic modulation of the signal. The light intensity at the detection unit is detected with, for example, a photomultiplier and the generated signal is analysed with a lock-in detection technique.

In this approach, the measurements are done at a single spot, and thus scanning the sample in a scanning optical microscope is required to obtain a two-dimensional map of the sample. After passing through the first polarizer, the light reflects from the semi-transparent mirror and then passes twice through the MOIF (getting reflected from the mirror at its bottom). Then the light beam passes through a Faraday modulator and, after passing the analyser, the light is detected by an intensity detection unit, such as a photomultiplier. The Faraday modulator comprises a MOIF sensor without a mirror layer placed inside a solenoid. A small AC current is driven through the solenoid producing a small (compared to the stray field of the studied samples) AC magnetic field in it. Due to the MOIF placed in the solenoid, this field results in a small periodic deviation of the light polarization in addition to the constant angle of rotation of the plane of polarization generated by the sample stray field acting on the sensor. The Faraday modulator acts as an analogue differentiator for the light intensity.

5.2.8 MOIF signal generation by a polarization camera

The measurement scheme for MOIF measurements with a polarization camera is shown in Figure 5 c).

The light is generated by a light source. After passing the polarizer, the incident light passes the sensor substrate and the MOIF, is reflected by the sensor reflecting layer and then passes the active layer a second time. The reflected light beam shows a Faraday rotation proportional to the local sensor magnetization M_z. The polarization is measured with an image sensor combined with a micro-polarizer array.

5.2.9 MOIF signal generation theory for direct MOIF measurements

The reflected light beam with intensity I^{refl} [Formula (4)] traverses the analyser. The transmitted intensity passing through the analyser as seen by the intensity detection unit, I^{det}, is described by Malus law:

$$I^{\text{det}} = I^{\text{refl}} \sin^2(\alpha + \theta) \tag{5}$$

where θ is the deviation of the angle of the analyser from the crossed position of polarizer and analyser.

5.2.10 Selecting the analyser operating angle

In a crossed geometry of analyser and polarizer, i.e. $\theta = 0$, H_z values with opposing signs would give the same signal which prevents an unambiguous assignment of the signal to the underlying H_z. Additionally, choosing $\theta = 0$ leads to low sensitivity in low fields (zero derivative). Therefore, for calibrated measurements, a value of $\theta \neq 0$ shall be chosen. The impact of angle θ between analyser and polarizer on the relation between intensity I^{det} at the detector and magnetic field is shown in Figure 6.

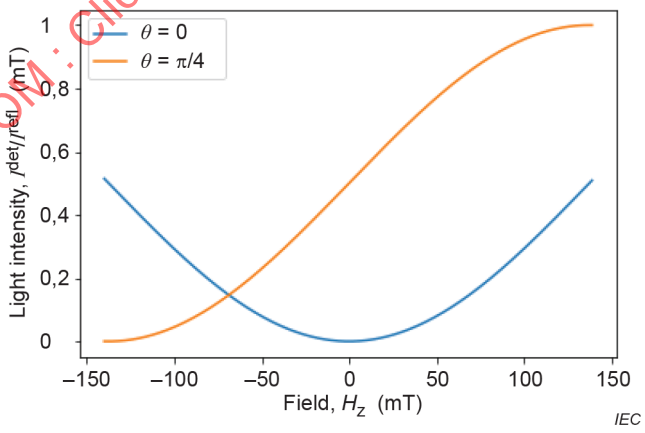

Figure 6 – Schematic representation of the impact of angle θ between analyser and polarizer on the relation between intensity I^{det} at the detector and magnetic field in the measurement plane H_z

5.2.11 MOIF signal generation theory in differential MOIF measurements

Since the incident beam path and the passage through the sensor are identical in differential MOIF measurements and direct measurement, the signal generation up to this point is described by the same Formulas [Formulas (3), (4), (5)]; however, in the Malus law an additional term has to be added that describes the effect of the Faraday modulation [34]. The Faraday modulator leads to an additional Faraday effect contribution of

$$\alpha^{\mathrm{mod}} = \alpha_0^{\mathrm{mod}} \sin(\omega t) \tag{6}$$

where ω is the angular frequency of the AC current driven through the solenoid of the Faraday modulator. For a crossed geometry of polarizer and analyser, i.e. $\theta = 0$, the Malus law, Formula (5), for the intensity at the detector is thus replaced with

$$I^{\mathrm{det}} = I^{\mathrm{refl}} \sin^2\left(\alpha + \alpha_0^{\mathrm{mod}} \sin(\omega t)\right) \tag{7}$$

For both α and α_0^{mod} Formula (5) can be linearized into the form

$$I^{\mathrm{det}} \approx I^{\mathrm{refl}}\left(\alpha^2 + \alpha^{\mathrm{mod2}} + 2\alpha\alpha^{\mathrm{mod}}\right) = I^{\mathrm{refl}}\left(\alpha^2 + \alpha_0^{\mathrm{mod2}} \sin(\omega t)^2 + 2\alpha\alpha_0^{\mathrm{mod}} \sin(\omega t)\right) \tag{8}$$

This signal has two harmonics at ω and 2ω with respect to the modulation frequency ω. The signal detected at the first harmonic $\sin(\omega t)$ is

$$I^{\mathrm{det},\omega} \approx 2 I^{\mathrm{refl}} \alpha \alpha_0^{\mathrm{mod}} \tag{9}$$

where the product of the factors $2I^{\mathrm{refl}}\alpha_0^{\mathrm{mod}}$ is a constant, and thus the measured signal is proportional to the Faraday rotation α generated by the sensor. Combining Formulas (4) and (9) gives

$$I^{\mathrm{det},\omega} \approx 4 I^{\mathrm{refl}} \alpha_0^{\mathrm{mod}} d^{\mathrm{MOIF}} v(\omega) M_z = K_1 M_z \tag{10}$$

Therefore, the signal measured is directly proportional to the perpendicular magnetization component of the sensor M_z.

5.2.12 MOIF signal generation theory in the polarization measurement using a polarization camera

Measurement of angle of rotation of the plane of polarization using the polarization camera can be done with a simple optical system and a single shot without the analyser [35]. The polarization camera is a camera with a structure that integrates an image sensor with a micropolarizer array consisting of multiple polarizers with different angles formed according to the pixel size. Since the micropolarizer array has polarizers in four directions with different rotation angles $\vartheta = \theta + 90° = (0°, 45°, 90°, 135°)$, four light intensity images can be acquired by collecting only the pixels in each direction of the image captured by the snapshot. From the four light intensities $\left(I_{0°}, I_{45°}, I_{90°}, I_{135°}\right)$ can be obtained the Stokes parameters, s_0, s_1, and s_2, for the polarization state of the light as

$$\begin{pmatrix} s_0 \\ s_1 \\ s_2 \end{pmatrix} = \begin{pmatrix} \left(I_{0°} + I_{45°} + I_{90°} + I_{135°}\right)/2 \\ I_{0°} - I_{90°} \\ I_{45°} - I_{135°} \end{pmatrix}.$$

Consequently, the Faraday rotation angle α can be obtained by

$$\alpha = \frac{1}{2}\tan^{-1}\left(\frac{s_2}{s_1}\right),$$

and the stray field can be calculated from α using Formula (4).

By measuring the Stokes parameters, stray fields thus can be quantitatively measured even if an optical setup or optical conditions are changed.

5.3 Ambient conditions during measurement

Ambient conditions key control characteristics are summarized in Table 3.

The environmental measurement temperature T^{env} shall be kept stable to ±1,5 K during the measurement since changes of temperature lead to thermal drift that can impact the precision of the positioning system.

Relative humidity RH shall be controlled to (50 ± 4) % relative humidity and relative humidity and environmental measurement temperature shall be documented including their variability during the measurement process.

Table 3 – Ambient conditions key control characteristics

Key control characteristic	Identifier	Typical value	Comment
Environmental measurement temperature	T^{env}	(23 ± 1,5) °C	Shall be kept within the specified range. The impact on the measurement depends on the setup.
Relative humidity	RH	(50 ± 4) %	Shall be kept within the specified range. The impact on the measurement depends on the setup.

6 Measurement procedure

6.1 Calibration of measurement equipment

6.1.1 Calibration of analyser-based MOIF measurements for purely perpendicular magnetic fields $H = H_z$

The measurement with the MOIF system results in a two-dimensional raw signal distribution $S(x,y)$. The calibration allows it to be converted into quantitative magnetic field $H_z(x,y)$ or flux density distribution data $B_z(x,y)$ of the sample at the measurement height. Several effects impact the relation between S and B_z that can be categorized in sensor related contributions on the one hand and light source and imaging system related contributions on the other hand.

6.1.2 Calibration approach for one pixel

Calibrating the setup means establishing a unique relation $H_z(S)$. This requires $S(H_z)$ to be unambiguously invertible. The MOIF calibration is performed by applying an external magnetic field with a purely perpendicular magnetic field component to the sensor in the finalized measurement geometry. In this case a calibration means to measures $S(H_z)$ at a sufficient number of grid points, i.e. N_{cal} signal values S_i are determined at N field values $H_{z,i}$ in the field range of interest for $i \in \{0 \ldots N\}$. This establishes the MOIF calibration array in perpendicular magnetic fields F^{cal}.

If, for example, the sensitivity of the detection unit is linear and θ is chosen as $\theta = \pi/4$, this leads to a generalized equation

$$S = A \sin^2(B H_z + \theta) + C$$

with three parameters. $S(H_z)$ is then fitted to the measured $S(H_z)$.

The relation $H_z(S)$ is then found from an inversion of the equation above for which an analytical form can be given:

$$H_z = \frac{\arcsin\left(a(I - C)/A\right) - \theta}{B}$$

In general cases, an appropriate fit function, e.g. a polynomial fit function, shall be chosen.

Figure 7 shows the experimentally measured calibration data together with a polynomial fit. In this case, the experimentally observed $S(H_z)$ relation is rendered well.

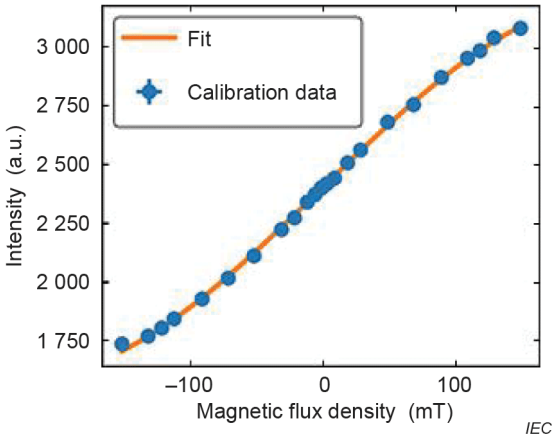

Figure 7 – Example of a calibration curve

6.1.3 Calibration approach for array sensors using an analyser-based detection scheme

For spot measurements, the calibration described above covers all calibration aspects.

In contrast, the sensitivity of a sensor array can show a dependence on the pixel position. Also, the illumination will typically not be homogeneous over the sensor area. As a consequence, the pixel dynamic of the detecting sensor can depend on the position on the sensor. This will translate into a pixel dependent relation $I(H_z)$ at the sensor which is translated into a signal by a pixel dependent $S(I)$ function. The calibration then shall be done for either each pixel of the array sensor or for a representative subset of the pixels which allows to find the calibration function of the other pixels by interpolation. This can be done in one of two ways. A dataset of the signal S detected by the detection system can be experimentally determined in appropriate units as a function of the applied out-of-plane external field H_z for all pixel indices (Nx, Ny). Alternatively, the same dataset is collected for only a (representative) subset of the sensor pixels and an interpolation approach is defined. As a result, for each pixel, a calibration function $F^{cal}(Nx, Ny)$ is given as an array for discrete values of $H_z(Nx, Ny)$ versus $S(Nx, Ny)$.

NOTE The determination of the calibration function $S(H_z)$ requires well-known stray fields; see, for example, [37]. When in large electromagnets the stray field will not be homogeneous over typical sensor dimensions of several centimetres. The field inhomogeneity shall be taken into account when calibrating the setup. Figure 9 shows the traceably characterized stray field distribution of an electromagnet with 25 cm pole diameter.

When $F^{cal}(Nx, Ny)$ is expected to change smoothly, the calibration array may be determined for only a representative subset of the MOIF pixels. The curve can show a hysteresis and shall be measured for a full field loop (0 A/m → $+H_{max}$ → $-H_{max}$ → $+H_{max}$). Here, H_{max} shall be chosen to be equal or larger than the maximum field for which the calibration shall hold.

6.1.4 Background image subtraction

Some MOIF measurement artefacts lead to an (approximately) constant parasitic background signal I^{BG} that is independent of the sample.

$$I^{det\prime} = I^{det} + I^{BG} \tag{11}$$

To reduce the impact of such unwanted signals, a background image is taken of the signal generated by the pure sensor without a sample (blank sensor image). The background image is subtracted from any sample measurement.

6.1.5 Calibration of differential MOIF for perpendicular magnetic fields $H = H_z$

Differential measurements are usually done as spot measurements since any sensor channel would necessitate lock-in detection. Here, the discussion of the calibration of differential MOIF measurements is limited to sample fields well below half the saturation field of the MOIF, $B^{SUT} < ½\ B^{SAT}$. For this situation, the effective field acting on the sensor magnetization with an in-plane uniaxial MOIF magnetic anisotropy field $B_{uoop} = \mu_0 \cdot H_{uoop}$ can be approximated as the sum of the external fields H_z, and H_x and a constant anisotropy field $H_A = H_{uoop}$. The sensor magnetization aligns with the effective field as shown in Figure 8.

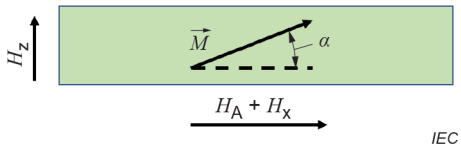

NOTE H_A is the anisotropy field of the MOIF.

Figure 8 – Angle of rotation of the plane of polarization of MOIF magnetization vector under an external magnetic field

The perpendicular magnetization component can be calculated from geometrical considerations.

$$M_z = \frac{H_z}{\sqrt{(H_A + H_x)^2 + {H_z}^2}} \tag{12}$$

For calibrations in purely perpendicular fields with $H_x = 0$, combining Formula (12) with Formula (10) gives the calibration equation for differential MOIF measurements.

$$\left|I^{det,\omega}\right| = K_1 \frac{H_z}{\sqrt{{H_A}^2 + {H_z}^2}} \tag{13}$$

$\left|I^{det,\omega}\right|$ is the measured lock-in amplitude. The parameter K_1 fully describes the signal generation and shall be determined from a calibration.

6.1.6 Calibration approach

Exploiting Formula (13) results in the following calibration approach, with is valid for sample field well below the H_{uoop}:

In the first step, as in direct MOIF measurements, a calibration array F^{cal} in perpendicular magnetic fields is taken for a full field loop (0 A/m → $+H_{max}$ → $-H_{max}$ → $+H_{max}$). For differential MOIF measurements, the signal recorded as a function of the external magnetic field is the lock-in amplitude $\left|I^{det,\omega}\right|$.

In the second step, the calibration array is fitted by the functional relation from Formula (13). The fitted parameter K_1 determines the calibration function.

The calibration approach for differential MOIF measurements thus reflects the calibration approach for direct MOIF measurement; however, the functional relation in between measured signal and magnetic field is assumed to be fixed as given by Formula (13).

6.1.7 Providing the perpendicular calibration field

6.1.7.1 General

The external magnetic field control characteristics are discussed in 6.1.7.2 to 6.1.7.5 and are summarized in Table 4.

6.1.7.2 Field homogeneity in z-direction

MOIF calibrations require well characterized calibration fields. Therefore, the magnetic field of the external magnetic field unit over the sensor volume shall be well defined. Typical macroscopic magnetic field generators like electromagnets can be expected to generate magnetic fields with a z-variation that is negligible over the sensor thickness. Consequently, only the spatial sensor coordinates (x,y) are regarded in describing the field homogeneity.

6.1.7.3 Field adjustability

The perpendicular magnetic field shall be adjustable in the calibration field range. Magnetic field units typically have a control parameter P which is an electric current for electromagnets or a distance for permanent magnets, and thus $H^{\text{ext}} = H^{\text{ext}}(P)$

6.1.7.4 Homogeneity of the perpendicular field component

In homogeneity considerations two aspects of the field inhomogeneity shall be taken into account. On the one hand, for any control parameter P, the z-component of the external field H_z^{ext} will show a spread as a function of the lateral position for any control parameter $H_z^{\text{ext}} = H_z^{\text{ext}}(p,x,y)$ which shall be regarded during the calibration.

6.1.7.5 Adverse in-plane field components

Additionally a spread in H_z^{ext} necessarily leads to the appearance of in-plane field components $H_{x,y}^{\text{ext}}(p,x,y)$. These in-plane fields impact the calibration to a degree that is hard to quantify, even if the spread of H_z^{ext} is taken into account. Therefore, a calibration magnet that provides a homogeneous $H_z^{\text{ext}}(p,x,y)$ shall be used.

Table 4 – External magnetic field control characteristics

Key control characteristic	Identifier	Typical value	Comment	Category
magnetic field unit control parameter	p	current, I = 1 A		instrument parameters
calibrated spatial distribution of the external magnetic field z-component	$H_z^{\text{ext}}(p,x,y)$			instrument parameters
calibrated spatial distribution of the external magnetic field in-plane component	$H_z^{\text{ext}}(p,x,y)$			instrument parameters

6.2 MOIF key control parameters

6.2.1 General

The MOIF setup key control characteristics are discussed in 6.2.2 to 6.2.9 and are summarized in Table 5.

6.2.2 Calibrated external magnetic field, H_z^{ext}

The calibration of the sensor requires the application of well-defined external magnetic fields $H_z^{ext}(x,y)$ generated by an external magnetic field unit, typically an electromagnet. The external magnetic field unit shall be well characterized and calibrated, in the sense that at any position of the sample a specified field value with a given uncertainty can be set. Figure 9 shows an example of a field distribution of a 25 cm diameter pole shoe electromagnet.

As can be seen in the field distribution plot, even large electromagnets may show field inhomogeneities that shall be regarded.

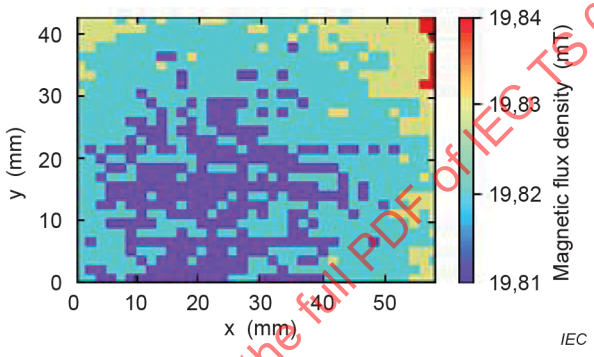

Figure 9 – Field distribution of a 25 cm diameter pole shoe electromagnet at 19,8 mT

The value for θ is chosen in such a way that $S(H_z)$ is monotonously increasing and sufficiently smooth over the setup calibration range.

6.2.3 Intensity of the light source

The intensity of the incident light beam is chosen in such a way that the detection range of the detection unit is well exploited.

6.2.4 Optical imaging geometry

The optical imaging geometry is chosen in such a way that the sample area of interest is imaged onto an array sensor area as large as possible to achieve highest lateral resolution in x and y.

6.2.5 Thickness of the MOIF, d^{MOIF}

The optimum thickness of the MOIF results from a trade-off between maximizing the Faraday signal and exploiting the dynamic range of the detection unit. Thicker MOIFs improve the Faraday of field components with large spatial wavelength and thus slow decay. However, field components with small spatial wavelengths decay rapidly and do not benefit from the sensor volume above their decay length. This reduces the signal amplitude ratio of small compared to large structures. Small amplitude ratios require a high dynamic range of the detector. Therefore, thicker sensors in general lead to a suppression of the signal of small structures.

6.2.6 Measurement height, h

The measurement height is defined in 3.3.3. In non-ideal samples, the MOIF roughness parameters and MOIF flatness parameters as well as the roughness and flatness of the sample contribute to the minimum measurement height.

6.2.7 Sensor measurement temperature, T^{sensor}

The temperature of the sensor T^{sensor} is typically higher than the environmental temperature due to the heating effect of the absorption of the incident beam in the sensor. The sensor temperature shall be stabilized before a calibrated measurement since samples have environmental temperature and cool down the sensor. The waiting time depends on the sample and the system.

6.2.8 Environmental measurement temperature, T^{env}

The environmental measurement temperature T^{env} impacts the optical properties of the magneto-optical measurement setup and its components. Calibrations are only valid for T^{env}.

6.2.9 Scan size $Sx \times Sy$ and pixel resolution Nx, Ny and pixel size $\Delta x \times \Delta x$

Scan size $Sx \times Sy$ and pixel resolution Nx, Ny (number of pixels in x- and y-directions) and thus the pixel sizes Δx and Δy are set by the user. They result from the elected magnification of the imaging optics and from the sensor array used as a detection unit.

Table 5 – MOIF setup key control characteristics

Key control characteristic	Identifier	Typical value	Comment	Category
MOIF sensor quality factor	Q		should be $Q < 1$ for calibrated stray field measurement	sensor parameter
thickness of the MOIF	d^{MOIF}	5 µm	shall be small compared to typical structure sizes	
MOIF reflective coating thickness	d^{rc}	3 µm	should provide sufficient reflectivity	
MOIF magnetic anisotropy field	$B_{uoop'}$	110 mT		
setup calibration range		±125 mT	approximately 20 % lower than B_{sat}	
saturation field	B_{sat}	160 mT		
MOIF protective coating thickness	d^{pc}	2 µm		
polarizer rotation angle	θ	45°		instrument parameter
image size pixel size pixel number	$Sx \times Sy$ $\Delta x \times \Delta y$ $Nx \times Ny$	18 mm × 13 mm 5 µm × 5 µm 4 140 × 2 884		
measurement height	h	3 µm	average distance of sample effective surface to MOIF nominal surface plane	measurement parameter
z-component of the magnetic field distribution of the sample under test	$H_z^{SUT}(x,y,z)$			sample data
measured raw data distribution	$S(x,y)$			measurement data

Key control characteristic	Identifier	Typical value	Comment	Category
external perpendicular magnetic field for calibration	$H_z^{ext}(x,y)$			setup data
MOIF calibration array in out-of-plane magnetic fields	$F^{cal}(Nx, Ny)$			calculated data

6.3 Detailed description of the measurement procedure

6.3.1 General

The measurement procedures for geometrical feature detection and calibrated magnetic field measurements are discussed in 6.3.2 to 6.3.10 and are summarized in Table 6 and Table 7.

6.3.2 Sample mounting

The SUT is mounted to the system in one of the following ways:

a) positioning it in the microscope and putting the sensor loosely onto the sample surface (with or without spacer);

b) pressing the sensor in a defined way onto the sample surface (with or without spacer);

c) positioning the sensor above the sample surface at a defined measurement height by any appropriate fixture.

In an inverted scheme, where the sample is placed onto the sensor, the sample is mounted in one of the following ways:

1) putting it loosely onto the sensor surface (with or without spacer);

2) pressing it in a defined way onto the sensor surface (with or without spacer);

3) positioning it above the sensor surface at a defined measurement height by any appropriate fixture.

6.3.3 Temperature stabilization

The sensor sensitivity depends on its temperature. The calibration is only valid for measurements that are performed at the sensor calibration temperature (within the given tolerances). After sample mounting an appropriate waiting time shall be observed to allow the sample and the system to stabilize so that the sensor measurement temperature T^{sensor} is constant during the calibration.

6.3.4 Frame averaging

Frame averaging (3.10.2) improves the signal-to-noise ratio but prolongs the data acquisition time. An appropriate number of averages N according to the specific measurement needs shall be chosen.

6.3.5 Background image

The differential raw data image is taken before the sample is mounted at a sensor measurement temperature T^{sensor} with the same number of averages N as selected for the sample. The background image measures residual intensities that are caused by imperfections of the setup and accounts for impacts of the sensor domain structure. The differential image is subtracted from any raw data image of the SUT.

6.3.6 Raw data distribution

After the temperature stabilization, an image of the SUT is taken with the chosen number of averages. The resulting image is the raw data distribution $S^{SUT}(x,y)$.

6.3.7 Measurement procedure for geometrical feature detection

The quantification of, for example, the characteristic dimensions requires (i) an adjustment of the MOIF setup and (ii) a measurement of the raw data distribution of the SUT.

The standardized sequence of measurement steps is as follows:

Adjustment of the MOIF setup

↓

Sample mounting and thermal stabilization

↓

Measurement of the raw data distribution of the SUT

6.3.8 Measurement procedure for calibrated magnetic field measurements (analyser based)

The quantification of stray fields by qMOIF (quantitative MFM) requires (i) an adjustment of the MOIF setup (ii) a calibration of the MOIF setup in well calibrated external magnetic field distribution, and (iii) a measurement of the raw data distribution of the SUT.

To ascertain that all key control parameters are well defined, the standardized sequence of measurement steps is as follows:

Adjustment of the MOIF setup

↓

Calibration of the MOIF setup

↓

Sample mounting and thermal stabilization

↓

Raw data measurement

↓

Calculation of calibrated stray field distribution

↓

Additional correction if required

6.3.9 Detailed description of the MOIF calibration procedure for quantitative stray field measurements

In the following, the procedure that shall be applied for the MOIF calibration for quantitative stray field measurements is described. It is summarized in Table 6.

1) Adjustment of the MOIF setup:
   a) A calibrated external magnetic field unit is provided that allows to apply well defined magnetic fields purely perpendicular to the MOIF nominal surface plane at the position of the sensor during the measurement.
   b) A MOIF setup imaging geometry is chosen that fits the characterization needs of the sample.
   c) A MOIF sensor is selected.
   d) A value for θ is chosen in such a way that $S(H_z)$ is monotonously increasing and sufficiently smooth over the setup calibration range.
   e) The intensity of the incoming light beam is chosen so that the detection unit is not overdriven for any field value in the setup calibration range. The light source remains continuously switched on.
2) Thermal stabilization:
   a) The environmental calibration temperature is set and stabilized.
   b) The sensor is allowed to reach thermal equilibrium. The equilibrium sensor calibration temperature is measured (including uncertainty).
3) Calibration data recording and analysis:
   a) The external magnetic field is looped in a specified number of steps. This can, for example, be done by a stepwise variation of the current if the external magnetic field unit is an electromagnet. If the step number is too low to adequately describe the $S(H_z)$ relation, the step number shall be increased. A loop of the magnetic field comprises the course $H_z^{ext} = 0 \rightarrow H_z^{ext,max} \rightarrow H_z^{ext,min} \rightarrow H_z^{ext,max}$ to detect possible hysteretic effects of the sensor. For each step the signal of the sensor is recorded. For an array sensor, the signal for a subset of the sensor pixels is recorded.
   b) The calibration measurement from step 3a) can be repeated and averaged to reduce type A uncertainties. The (averaged) data of step 3a) establish the MOIF calibration array in out-of-plane magnetic fields $F^{cal}(Nx, Ny)$.
   c) As the last step of the calibration interpolation rules for the MOIF calibration array in out-of-plane magnetic fields $F^{cal}(Nx, Ny)$ is are formulated, that allow to assign a unique H_z value to any signal within the range of signals for which step 3a) has been performed and for any pixel of the array sensor. This establishes the MOIF calibration curve in out-of-plane magnetic fields $F^{cal,fit}(Nx, Ny)$.

Table 6 – MOIF calibration protocol

Step	Action	Illustration	
1a	An external magnetic field unit with calibrated magnetic field distribution is provided	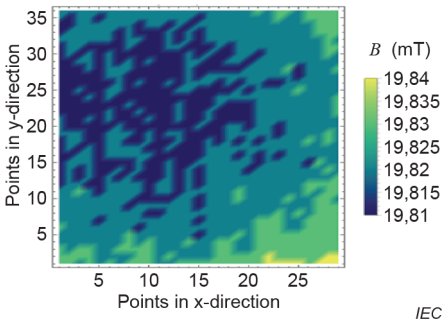 EXAMPLE: homogeneity of magnetic flux density of an electromagnet over an area of (60 × 70) mm^2 in the middle of the pole shoe at a current of 1,5 A.	required
1b	The setup imaging geometry is defined	EXAMPLE: wide field imaging geometry	required
1c	A MOIF sensor is selected	EXAMPLE: d^{MOIF} = 5 µm setup calibration range: ±125 mT $\mu_0 H_{\mathrm{sat}}$ = 160 mT ΔA = 5 µm × 5 µm Q < 1	required
1d	An analyser rotation angle is chosen	EXAMPLE: θ = 45°	required
1e	The intensity of the incident beam is adjusted	EXAMPLE: $I^{\mathrm{inc}} = I_0$	required
2a	Environmental calibration temperature is stabilized	EXAMPLE: $T^{\mathrm{cal,env}}$ = 23 °C	required
2b	The sensor temperature is allowed to reach equilibrium	EXAMPLE: $T^{\mathrm{cal,sens}}$ = 23 °C	required
3a	A calibration array for each field value and pixel of the array sensor is recorded	EXAMPLE: $F^{\mathrm{cal,exp}}(Nx, Ny) \geq S(x,y)$ for H_z^{ext} = 70 mT 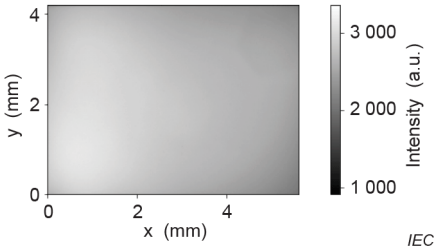	required
3b	The calibration measurement from step 3a)can be repeated	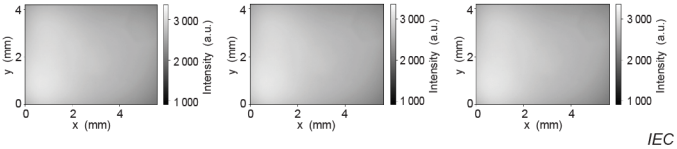	optional

Step	Action	Illustration	
3c	Interpolation rules for the MOIF are formulated	$F^{cal,fit}(Nx, Ny) => S(x,y) = k_1(x,y)+k_2(x,y)\ (a\ H_z^3 + b\ H_z)$ 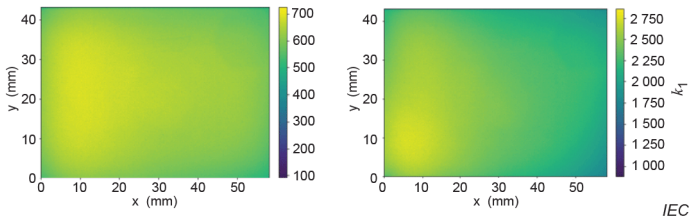 EXAMPLE: interpolation rules in the form of polynomial fit parameters for a spatially dependent third order polynomial relation between H_z and detector signal S. Parameters a and b are functions of the sensor anisotropy.	required

6.3.10 Detailed description of the MOIF calibrated stray field measurement procedure

In the following, measurement procedure that shall be applied to calibrated stray field measurements is described. It is summarized in Table 7

1) Adjustment of the MOIF setup as described in 6.3.8, step 1).
2) Calibration of the MOIF setup as described in 6.3.8, step 3).
3) Background image recording.
4) Sample mounting and thermal stabilization:
   a) The sample under test is positioned on the sensor.
   b) The sensor is allowed to reach thermal equilibrium. The equilibrium sensor measurement temperature is measured (including uncertainty).
5) Measurement of raw data distribution:
   a) The SUT raw data distribution $S^{SUT}(Nx, Ny)$ is measured.
   b) The SUT measurement from step 5a) can be repeated and averaged to reduce type A uncertainties. The (averaged) data of step 5a) establish the MOIF calibration array in out-of-plane magnetic fields $F^{cal}(Nx, Ny)$.
6) Calculation of a calibrated stray field distribution. As the last step, calibrated stray field data are calculated for each pixel from the SUT raw data from step 5 by applying the MOIF calibration curve in out-of-plane magnetic fields $F^{cal,fit}(Nx, Ny)$.

Table 7 – Calibrated stray field measurement procedure

Step	Action	Illustration	
1	Adjustment of the MOIF setup		
2	Calibration of the MOIF setup		

Step	Action	Illustration	
3	A background image is recorded	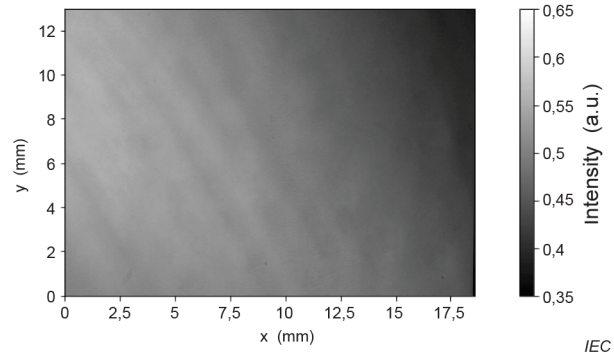	
4a)	A sample under test is mounted and allowed to reach thermal equilibrium	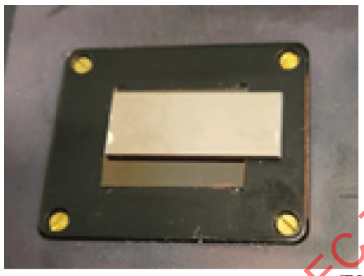	
4b)	Environmental temperature is stabilized and the sensor temperature is allowed to reach equilibrium	$T^{cal,env}$ = 23 °C $T^{cal,sens}$ = 32 °C	required
5	A signal distribution is recorded and the background image is subtracted	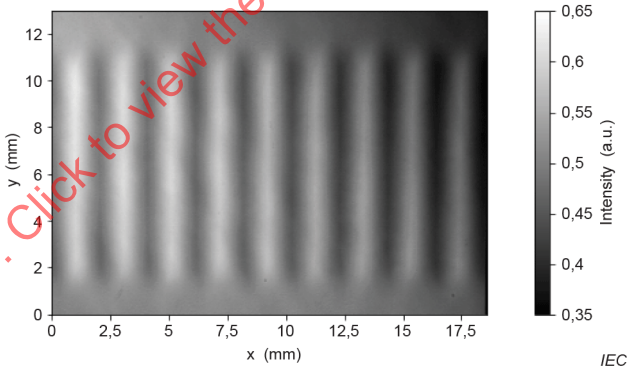	
6	Calculation of the calibrated raw magnetic field distribution of a magnetic sample, H_z^{raw}	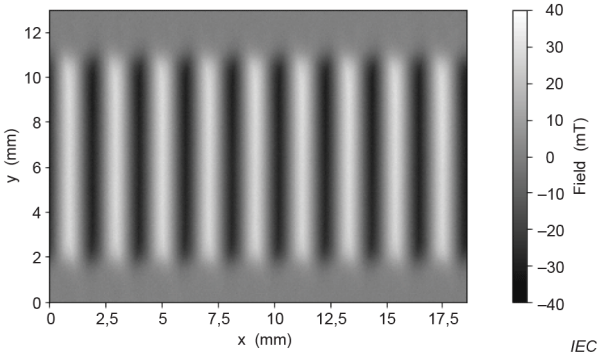	

6.4 Measurement accuracy

6.4.1 Contribution of in-plane magnetic field components

The perpendicular magnetization component, which determines the sensor's Faraday rotation, M_z, is not only defined by the perpendicular component of the sample stray field but results from the interplay between the vectorial field components (H_x, H_y, H_z) and the magnetic anisotropies of the indicator film. For MOIF with uniaxial anisotropy, properties are symmetric with respect to the z-axis, and thus, in 6.4.2, H_x is used for any in-plane magnetic field.

6.4.2 In-plane magnetic fields contribution for low magnetic fields $H << H_{uoop}$

In the frame of the approximations discussed for differential MOIF measurements, both field components H_z and H_x can be found for a calibrated measurement [34]. The approach is based on the application of a small bias field in the in-plane x-direction, ΔH_x, and a measurement of the change in the signal ΔS. For hard magnetic samples, the sample magnetization is not affected by ΔH_x, and the change in the signal ΔS can solely be attributed to the declination of the MOIF magnetization vector. This allows the derivative of the signal to be measured with respect to H_x, $\partial I/\partial H_x$.

This derivative can also analytically be expressed based on Formula (12), but now also considering in-plane components, as

$$\left|I^{\det,\omega}\right| = K_1 \frac{H_z}{\sqrt{\left(H_A + H_x\right)^2 + {H_z}^2}} \tag{14}$$

$$\frac{\partial\left|I^{\det,\omega}\right|}{\partial H_x} = -K_1 \frac{H_z\left(H_A + H_x\right)^2}{\left(\left(H_A + H_x\right)^2 + {H_z}^2\right)^{-3/2}} \tag{15}$$

Combining Formulas (12) and (13) gives a system of two equations with two unknowns which can be solved for H_x and H_z. The prefactor K_1 is known from calibrations in perpendicular external magnetic fields. As described above, $\frac{\partial\left|I^{\det,\omega}\right|}{\partial H_x}$ can be approximated by applying small bias fields. This approach is not applicable to soft magnetic samples. It can be shown [34], that for a low sample stray field strength, the effect of H_x on the magneto-optical signal can be neglected. The measured signal S then can with minor error directly be related to H_z data as derived from the calibration curve in perpendicular magnetic fields.

6.4.3 In-plane magnetic field contribution for fields in the order of magnitude of H_{uoop}

For magnetic fields in the order of magnitude of H_{uoop}, in-plane field components increasingly contribute to the measured signal. To estimate the impact, the signal as measured with a calibrated system was simulated and compared to the signal that would be measured if the MOIF would only see the respective perpendicular field component. The simulations were performed for magnetic field vectors with varying orientation but constant field amplitude H_{amp}, and thus normalized amplitude $h_{amp} = H_{amp}/H_{uoop}$. Figure 10 shows plots of the simulated measured (blue) MOIF signal compared with the signal expected for pure h_z, for all values $h_z = H_z/H_{uoop}$ that can be observed for a given h_{amp}. The measured MOIF signal in all cases underestimates the actual value, since the additional in-plane field component slightly rotates the MOIF magnetization back into the sensor plane. For any field vector with an amplitude which is smaller than the chosen h_{amp}, the deviation is lower. Whereas for $h_{amp} = 0,1$ the deviation is small, it gets significant for $h_{amp} = 0,5$.

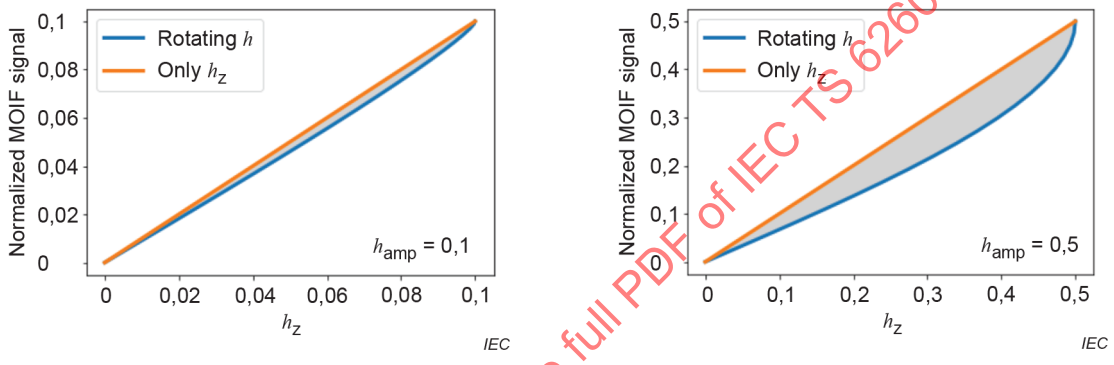

Figure 10 – Impact of high in-plane components on the measured MOIF signal

6.4.4 Forward simulation

In general cases, where the approximations from above are not valid, a unique solution for the inversion problem $S(H_z)$ cannot be calculated. However, the sensor signals S can be forward simulated by numerically determining the minima of the free energy function of the MOIF material for each given H. When multiple minima are found, the solution closest to the solutions found for neighbouring sample positions shall be selected to enforce continuity. The applied free energy function considers the magnetic anisotropies neglecting spurious uniaxial in-plane anisotropy contribution.

The approach is further detailed in Annex A.

6.4.5 Influence of the finite sensor thickness

The finite sensor thickness leads to an averaging of the field over the sensor. Stray field components of smaller structures decay faster with increasing distance from the sample. Figure 11 shows this on the example of a magnetic scale with two different pole widths and periodically written poles.

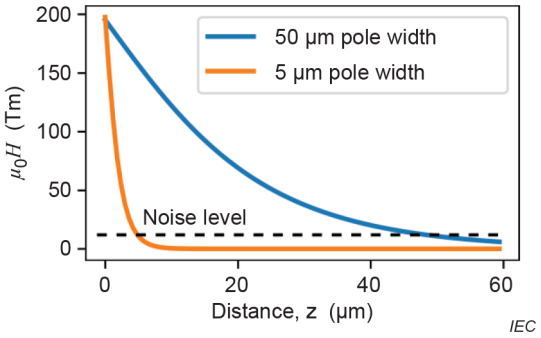

Figure 11 – Decay behaviour of H_z as a function of the pole width for magnetic scales with a periodic magnetic pole pattern

For structures so small that the stray fields decay significantly over the sensor thickness, the sensor measures a reduced signal compared to the field present at the sample-side face of the sensor.

6.4.6 Transfer function-based sensor thickness correction

The impact of the finite MOIF sensor thickness can be calculated as multiplication of the Fourier transform of H_z at the MOIF nominal surface plane, i.e. at the measurement height h = 0, $H(k, h=0)$, with a transfer function $\mathrm{TF}^{\mathrm{MOIF}}$ which returns the thickness averaged stray field $H^{\mathrm{avg}}(x,y)$.

$$\mathrm{TF}^{\mathrm{MOIF}} = \frac{1-e^{-kD}}{kD}, \quad \text{and thus} \quad H^{\mathrm{avg}}(k) = H(k, h=0) \times \mathrm{TF}^{\mathrm{MOIF}} \tag{16}$$

Details can be found in Clause A.5.

6.4.7 Spatial resolution

6.4.7.1 Sensor array limited resolution

The lateral resolution in x and y is limited by the pixel size of the sensor array.

6.4.8 Diffraction limited resolution

In microscopy setups with very thin sensors, the lateral resolution in x and y is limited by the wavelength of the light source due to the optical diffraction limit.

6.4.9 Sensor thickness limited resolution

The magnetic field of structures with small spatial wavelengths decays faster with the distance from the sample surface than the field of structures with large spatial wavelengths. As a consequence, for structure in the size of the sensor thickness, a significant stray field decay over the sensor can occur, which leads to a lower net Faraday effect for identical field amplitudes due to an averaging over the sensor thickness. This can be compensated by a higher dynamic range of the detection unit. Otherwise, it leads to a noise level induced cut-off frequency for small structures.

6.4.10 Signal generation artefacts in MOIF measurements

Artefacts in MOIF are mostly caused by imperfections of the sensor, inhomogeneities of the detection unit array sensor and by optical components with a finite Verdet constant which show a Faraday effect. Most artefacts are implicitly corrected by the sensor calibration.

A detailed discussion can be found in Clause A.6.

6.4.11 Uncertainty evaluation

When performing a calibrated field measurement of a sample under test, the uncertainties of the different calibration steps enter into the uncertainty budget and shall be recorded for a quantitative analysis.

6.4.12 Calibration uncertainty

The uncertainty evaluation of the F^{cal} considers type A and type B components.

Type A uncertainty is induced by noise in the measured raw data distributions.

Type B uncertainty consists of contributions from:

– magnetic field during the calibration measurement, H_z^{cal};
– measurement height, h;
– sensor calibration temperature, $T^{\mathrm{cal,sens}}$;
– environmental calibration temperature, $T^{\mathrm{cal,env}}$;
– sensor thickness, d^{MOIF};
– pixel size, ΔA.

6.4.13 Uncertainty of calibrated field measurement

The uncertainty evaluation of the F^{cal} considers type A and type B components.

Type A uncertainty is induced by noise in the measured SUT raw data distribution (here: sensor signal) and can be estimated by averaging data from independent calibrated measurements of the SUT.

Type B uncertainty consists of:

– uncertainties of key control parameters: pixel size, measurement height, sensor thickness;
– the uncertainty of the calibration function.

Key control characteristics that are not changed between calibration and calibrated measurements cancel out in the Type B uncertainty and only affect the Type A uncertainty. The uncertainty evaluation key control characteristics are summarized in Table 8.

Table 8 – Uncertainty evaluation key control characteristics

Key control characteristic	Identifier	Typical value	Relevance
Uncertainties contributions for the determination of the calibration function			
sensor calibration temperature, $T^{\mathrm{cal,sens}}$	$uT^{\mathrm{cal,sens}}$,	1°	high
environmental calibration temperature, $T^{\mathrm{cal,env}}$	$uT^{\mathrm{cal,env}}$	1°	high
calibration field, H_z^{cal}	uH_z^{cal}	2 mT	low
measurement height, h	uh	2 µm	high
sensor thickness	ud^{MOIF}	100 nm	low
pixel size	$u\Delta A$	0,01 µm^2	high
Uncertainty contributions for calibrated stray field measurement			
calibration function, $F^{\mathrm{cal,fit}}(Nx, Ny)$	$uF^{\mathrm{cal,fit}}$	10 %	high
sensor calibration temperature, $T^{\mathrm{cal,sens}}$	$uT^{\mathrm{cal,sens}}$	1°	high
environmental calibration temperature, $T^{\mathrm{cal,env}}$	$uT^{\mathrm{cal,env}}$	1°	high
calibration field, H_z^{cal}	uH_z^{cal}	2 mT	low
measurement height, h	uh	2 µm	high
sensor thickness, d^{MOIF}	ud^{MOIF}	0,1 µm	low

For uncertainty evaluations and propagation, refer to ISO/IEC Guide 98-3 [36].

7 Data analysis and interpretation of results

7.1 Quantitative data analysis

A quantitative data analysis can be performed by any software implementing the required and discussed step.

7.2 Secondary parameters from MOIF measurements

7.2.1 General

Material parameters of interest typically are secondary parameters which are derived from the magnetic field distribution of the sample under test, $H_z^{\mathrm{SUT}}(x,y,z)$, by appropriate analysis techniques. Relating these parameters to the $H_z^{\mathrm{SUT}}(x,y,z)$ distribution of the sample makes them traceable to the SI system. Examples for materials where secondary parameters are of interest are magnetic scales – see, for example, [37] and Annex C – and magnetic sheets, see Annex C.

7.2.2 Secondary parameters of magnetic scales

Magnetic scales in the form of pole rings and linear scales form an active magnetic measurement system in combination with the sensors. Relevant parameters are, for example, defined in DIN SPEC 91411. Geometric and magnetic parameters eventually shall be traced back to spatially resolved field measurements as can be performed by calibrated MOIF. Such parameters are, for example, the magnetic period, nominal flux density and its deviation, and the magnetic pole width with deviation, as well as the scales accuracy.

7.2.3 Secondary parameters of grain-oriented electrical steel sheets

Grain-oriented steel sheets are an important material in the production of energy efficient transformers and of large, high-performance generators. They are tailored to produce specific magnetic properties like small hysteresis area resulting in low power loss per cycle, low core loss, and high permeability. The performance of the grain-oriented electrical steel sheets eventually depends on the grain sizes and the spread of orientations as well as on the grain remagnetization behaviour under varying flux density. Such characteristics can be assessed by MOIF in feature detection mode.

8 Results to be reported

8.1 Cover sheet

The results of the measurement shall be documented in a measurement report, including the date and time of the measurement as well as the name and signature of the person responsible for the accuracy of the report.

8.2 Product / sample identification

The report shall contain all information to identify the test sample and trace back the history of the sample:

– general procurement information;
– general material description top view, indicating the inspected area and location of the measurement positions.

8.3 Measurement conditions

The laboratory ambient conditions during the test:

– environmental measurement temperature (for example, 23 °C ± 1,5 °C);
– relative humidity (for example, (50 ± 4) %).

8.4 Measurement specific information (examples)

– number of frame averages used (e.g. 30);
– instrument;
– MOIF and sensor producer, type name, sensor properties;
– calibration status of equipment.

8.5 Measurement results

– Sampling plan used. For example,
  • coordinate system used in the magneto-optical measurement setup in absolute positions with a definition of the origin so that the measurement locations can be related to the technical drawing of the sample.
– Results of the stray field distribution measured according to this document. For example,
  • table of mean values and standard deviation of the stray field distribution measured according to this document at the positions defined by the sampling plan,
  • colour maps for the stray field distribution measured according to this document. The colour map shall be scaled in absolute positions in respect of the origin of the coordinate system. The colour code should be calibrated in absolute values of the measured stray field distribution.

Annex A
(informative)

Supporting information

A.1 Mathematical basics

A.1.1 Continuous Fourier transform versus discrete Fourier transform

The continuous Fourier transform $F(k_x,k_y)$ of a two-dimensional function $f(x,y)$ is defined as

$$F\left(k_x,k_y\right)=\iint f\left(x,y\right)e^{-ik_x x-ik_y y}\mathrm{d}x\mathrm{d}y\ .$$

However, MOIF data typically are taken at discrete sampling points in the form of a pixel image $f^{\mathrm{D}}(x,y)$ with a pixel number $Nx \times Ny$ over an image size $Sx \times Sy$. The resulting pixel size $\Delta x \times \Delta y$ can be calculated from $\Delta x = Sx/Nx$ and $\Delta y = Sy/Ny$.

NOTE Different MOIF systems can have different definitions of Δx, Δy, Sx, Sy, Nx and Ny.

The discrete Fourier transform $F(u,v)_{\mathrm{DFFT}}$ on $f^{\mathrm{D}}(m,n)$ is defined as

$$F\left(k,l\right)_{\mathrm{DFFT}}=\sum_{m=0}^{Nx-1}\sum_{n=0}^{Ny-1}f^{\mathrm{D}}\left(m,n\right)e^{-2\pi i\left(\frac{mk}{Nx}+\frac{nl}{Ny}\right)}\ \text{with}\ k\in\left\{0,1,\ldots Nx-1\right\}\ ,l\in\left\{0,1,\ldots Ny-1\right\}\qquad(A.1)$$

The corresponding wave vectors k_x and k_y that are used further below for field calculations can be calculated from the pixel dimensions in k-space dk_x and dk_y. mod is the modulo operator.

$$dk_x=\frac{2\pi}{Nx\,\Delta x}=\frac{2\pi}{Sx}\qquad k_x\left(u\right)=\left(\left(u+\frac{Nx}{2}\right)\mathrm{mod}\,Nx-\frac{Nx}{2}\right)\times dk_x$$

$$dk_y=\frac{2\pi}{Ny\,\Delta y}=\frac{2\pi}{Sy}\qquad k_y\left(u\right)=\left(\left(u+\frac{Ny}{2}\right)\mathrm{mod}\,Ny-\frac{Ny}{2}\right)\times dk_y$$

A.1.2 Partial (two-dimensional) Fourier space

The partial two-dimensional Fourier transform $F(k,z)$ of a function $f(r,z)$ is defined as

$$F\left(k,z\right)=\iint f\left(r,z\right)e^{-ik_x x-ik_y y}\,\mathrm{d}x\,\mathrm{d}y\qquad(A.2)$$

where $k = (k_x,k_y)$ and $r = (x,y)$.

A.1.3 Cross correlation theorem

A cross-correlation $f * g$ between two functions f and g is defined as

$$f(t) * g(t) = \int f(\tau) g(t+\tau) \mathrm{d}\tau$$

The Fourier transform of a cross-correlation product is

$$F(f * g) = F^* \times G \tag{A.3}$$

Where the asterisk * denotes the complex conjugate and capital letters denote the Fourier transform.

A.2 Pseudo-Wiener filter

A.2.1 Pseudo-Wiener filter-based deconvolution process

The Pseudo-Wiener filter implements a regularized deconvolution in the form

$$G(k,z) = H(k,z) F(k,z)$$

and thus

$$F(k,z) = G(k,z) \frac{H^*(k,z)}{|H(k,z)|^2 + \alpha}$$

α can be calculated from an L-curve criterion.

A.2.2 L-curve criterion

The L-curve criterion allows to find a unique regularization parameter α to be used in the pseudo-Wiener deconvolution approach. It mediates between the two contrary aspects, low residual norm $\|HF - G\|_2$ and low norm $\|F\|_2$. The L-curve is the L-shaped plot of $\|F\|_2$ versus $\|HF - G\|_2$.

A.3 Magnetic fields in partial Fourier space

A.3.1 Differentiation in partial Fourier space

In a region in which the magnetic field is rotation free, the partial Fourier space Nabla operator ∇ becomes

$$\nabla(k) = \nabla_k = \left(ik_x\ , ik_y\ , -k\right) \tag{A.4}$$

where $k = \sqrt{k_x^2 + k_y^2}$.

A.3.2 Magnetic fields in partial Fourier space

In two-dimensional partial Fourier space and in a region where the magnetic field is rotation free, all components of the field vector H can be calculated from its z-component

$$H(k,z) = -\frac{1}{k}\nabla_k H_z(k,z), \tag{A.5}$$

and thus

$$H_z(k,z) = H_z(k,z')e^{-ik(z-z')} \tag{A.6}$$

A.4 Calculating the equilibrium magnetization of uniaxial in-plane MOIF sensors in external magnetic fields

A.4.1 Solving the free energy equation

To describe the behaviour of the MOIF magnetization vector M in the MOIF as a function of an external field, we consider its energy density functional. The energy density of the MOIF film is a sum of the demagnetization energy f_{demag}, the Zeeman energy f_{zee} of the magnetization in the external field and an energy term caused by the uniaxial anisotropy f_{uni}, with the anisotropy axis in z-direction and with a negative MOIF magnetic anisotropy constant K_{uoop} (easy plane x-y). Higher order anisotropy terms are neglected.

$$f_{\text{demag}} = -\frac{1}{2}\mu_0 M_S{}^2\left(N_x m_x{}^2 + N_y m_y{}^2 + N_z m_z{}^2\right)$$

$$f_{\text{zee}} = -\mu_0 M_S\left(m_x H_x + m_y H_y + m_z H_z\right))$$

$$f_{\text{uni}} = K_u \sin^2(\theta)$$

Here, $m = (m_x, m_y, m_z)$ is the MOIF normalized magnetization vector $m = \frac{M}{M_S}$. The external field is $H = (H_x, H_y, H_z)$ and θ is the angle between M and the anisotropy axis e_z.

Since the problem shows rotational symmetry with respect to the z-axis, the external magnetic field can be assumed to lie in the x-z-plane, without a loss of generality. For thin films, like the MOIF sensor, the demagnetization-Tensor takes the values $N_x = 0$, $N_y = 0$ and $N_z = -1$.

The total energy density is thus given by

$$f_{\text{tot}} = f_{\text{zee}} + f_{\text{demag}} + f_{\text{uni}} = -\mu_0 M_S\left(m_x H_x + m_z H_z\right) - \frac{1}{2}\mu_0 M_S{}^2 m_z{}^2 + K_u \sin^2(\theta)$$

The effective field H_{eff} determines the equilibrium direction of the magnetization. It can be calculated from f_{tot} by calculating its vectorial derivative with respect to m:

$$H_{\text{eff}} = -\frac{1}{\mu_0 M_S}\frac{\partial f_{\text{tot}}}{\partial m}$$

For $f_{\text{tot}} = f_{\text{zee}} + f_{\text{uni}}$ this results in

$$H_{\text{eff}} = H - M_S m_z e_x + \frac{1}{\mu_0 M_S}\frac{\partial}{\partial m} K_u \sin^2(\theta)$$

e_x, e_y, e_z are unit vectors along the respective axes.

Exploiting $m_x = \sin(\theta)\cos\cos(\varphi)$ and $m_y = \sin(\theta)\sin\sin(\varphi)$, where φ is the azimuthal angle of M in the x-y-plane, and thus $m_x{}^2 + m_y{}^2 = \sin^2(\theta)(\varphi) + \sin^2(\theta)(\varphi) = \sin^2(\theta)$, one gets

$$H_{\text{eff}} = H + \frac{2K_u}{\mu_0 M_S}\sin(\theta) \times e_x = H - H_d \cos(\theta) + H_a \sin(\theta)$$

Or, if expressed by the polar angle θ,

$$H_{\text{eff}} = H + \frac{2K_u}{\mu_0 M_S}\sin(\theta) \times e_x = H - H_d \cos(\theta) + H_a \sin(\theta)$$

For an easy-plane anisotropy with negative K_u, the MOIF magnetic anisotropy field $H_a = -\frac{2K_u}{\mu_0 M_S} e_x$ points in the positive e_x-direction. The demagnetization field $H_d = -M_S e_z$ points in the negative e_x-direction.

For low external fields, the sensor magnetization is only slightly declined from the equilibrium direction and $\theta \approx \frac{\pi}{2}$ and thus $\sin(\theta) \approx 1$ and $\cos(\theta) \approx 0$. As a consequence, for low fields, a low field approximation for the effective field can be employed:

$$H_{\text{eff}}^{\text{lowfield}} = H + H_a$$

For higher field, the equilibrium magnetization in perpendicular fields $H_x = 0$ can be found by determining the minimum of the free energy function f_{tot}, with respect to the polar magnetization angle, i.e. by solving $\frac{\partial f_{\text{tot}}}{\partial \theta} = 0$.

$$\frac{\partial f_{\text{tot}}}{\partial \theta} = -\frac{\partial}{\partial \theta}(\mu_0 M_S m_z H_z - \frac{1}{2}\mu_0 M_S{}^2 m_z{}^2 + K_u \sin^2(\theta))$$

$$= \frac{\partial}{\partial \theta}(-\mu_0 M_S \cos\theta H_z - \frac{1}{2}\mu_0 M_S{}^2 \cos^2\theta + K_u \sin^2(\theta))$$

$$= \mu_0 M_S \sin\theta H_z + \mu_0 {M_S}^2 \cos\theta \sin\theta + 2K_u \cos\theta \sin\theta$$

$$= \sin\theta \left(\mu_0 M_S H_z + \mu_0 {M_S}^2 \cos\theta + 2K_u \cos\theta \right) \equiv 0$$

Since $\sin\theta = 0$ does not fulfil the requirement of a $\frac{\partial^2 f_{\text{tot}}}{\partial^2} > 0$, the second factor leads to the solution.

$$\cos\theta = \frac{H_z}{M_S + \frac{2K_u}{\mu_0 M_S}} = \frac{H_z}{M_S + H_a} = \frac{H_z}{H_a'},$$

where H_a' is an effective anisotropy field that includes the demagnetization field. As can be seen from this formula, for a uniaxial anisotropy and purely perpendicular fields H_z, the MOIF perpendicular magnetization component $M_z = m_z M_S = M_S \cos\theta$ increases linearly with H_z until $H_z = H_a'$, where the material reaches saturation at the effective anisotropy field.

A.4.2 Determination of the anisotropy constants of the sensor active material

The magnetic anisotropy constants of a MOIF sensor can be characterized by ferromagnetic resonance (FMR) measurements [37]. To this end, the sample is placed upside down onto a coplanar waveguide (CPW) that is connected to a vector network analyser (VNA). Then, an in-plane magnetic field with constant amplitude, high enough to essentially align the sensor magnetization with the field (e.g. 100 mT) is applied and rotated in the plane around the MOIF to perform φ-scans. The VNA detected transmission parameter S_{21} is monitored for absorption analysis.

Figure A.1 shows the angular dependence of the FMR spectra. The dispersion relation of the homogeneous mode, the perpendicular standing spin wave mode, $k = 0$, which is a homogeneous, spatially independent excitation, can be derived from the Landau-Lifshitz-Gilbert equation without knowledge on the materials exchange constant A, unlike for the higher k modes. For the analysis of the FMR data, the spectra were modelled following the Smit-Beljers-Suhl approach that relates the ferromagnetic resonance frequency $f = \frac{\omega}{2\pi}$ of the material to the derivatives of the magnetization and field dependent terms of the free energy function F of the material:

$$\frac{\omega}{\gamma} = \frac{\partial^2 F}{\partial \theta^2} \sqrt{\frac{\partial^2 F}{\partial \theta^2} \times \frac{\partial^2 F}{\partial \varphi^2} - \left(\frac{\partial^2 F}{\partial \theta \partial \varphi} \right)^2}, \gamma = \frac{g\mu_B}{\hbar}. \tag{A.7}$$

Where the derivatives is taken at the equilibrium magnetization angles θ_0 (to the plane normal) and φ_0 (in the plane). γ is the gyromagnetic ratio and g the g-factor. In the MOIF magnetic thin film material, the dominant contributions to F are the Zeeman energy F_{zee}, the demagnetization energy F_{demag} and the crystalline anisotropy energy terms F_{c} (cubic anisotropy), F_{uip} (uniaxial in-plane anisotropy), and F_{uoop} (out-of-plane uniaxial anisotropy). All contributions are functions of the magnetic field H and the magnetization M vectors. For convenience, both vectors are given in spherical coordinates.